Role of π-conjugation on the coordination behaviour, substitution kinetics, DNA/BSA interactions, and *in vitro* cytotoxicity of carboxamide palladium(II) complexes

Reinner O. Omondi[a], Nicole RS. Sibuyi[b], Adewale O. Fadaka[b], Mervin Meyer[b], Deogratius Jaganyi[c,d], Stephen O. Ojwach*[a]

[a]*School of Chemistry and Physics, University of KwaZulu-Natal, Private Bag X01, Scottsville, Pietermaritzburg 3209, South Africa.*
[b]*Department of Biotechnology, University of the Western Cape, Bag X17, Bellville, 7535, Cape Town, South Africa.*
[c]*School of Pure and Applied Sciences, Mount Kenya University, P.O. Box 342-01000, Thika, Kenya.*
[d]*Department of Chemistry, Faculty of Applied Sciences, Durban University of Technology, P.O. Box 1334, Durban 4000, South Africa.*

Table of Contents

1.0 Synthesis of ligands

1.1. N-(pyridin-2-ylmethyl)pyrazine-2-carboxamide (L_1)

To a solution of pyrazine-2-carboxylic acid (0.62 g, 5.00 mmol) and 2-picolylamine (0.54 g, 5.00 mmol) in pyridine (15 mL) was slowly added triphenyl phosphite (1.55 g, 5.00 mmol) for 15 min. The reaction mixture was refluxed at 100 °C for 12 h. The mixture was cooled to room temperature and poured into ice-cold water (40 mL). The resulting dark brown precipitate was collected by suction filtration, washed with copious amount of cold methanol and dried. Yield: 0.81 g (76%). ^{1}H NMR (400 MHz, DMSO-d_6): δ_H (ppm): 4.66 (d, $^3J_{HH}$ = 6.0, 2H, CH_2); 7.28 (dd, $^3J_{HH}$ = 6.0, 1H,

pyridine); 7.36 (d, $^3J_{HH}$ = 7.9, 1H, pyridine); 7.74 -7.79 (m, 1H, pyridine); 8.54 (d, $^3J_{HH}$ = 4.7, 1H, pyridine); 8.78 (t, $^3J_{HH}$ = 3.9, 1H, pyrazine); 8.91 (d, $^3J_{HH}$ = 2.5, 1H, pyrazine); 9.24 (d, J_{HH} = 1.4, 1H, pyrazine); 9.47 (t, $^3J_{HH}$ = 5.5, 1H, NH). ^{13}C NMR (DMSO-d6): δC (ppm): 44.16 (CH_2); 121.06 (CH, pyridine); 122.17 (CH, pyridine); 136.73 (CH, pyridine); 143.43 (CH, pyridine); 143.52 (CH, pyrazine); 144.61 (CH, pyrazine); 147.64 (CH, pyrazine); 148.81 (C, pyrazine); 157.65 (C, pyridine); 163.06 (C=O). FT-IR (cm^{-1}): υ(N-H) = 3313; υ(C=O) =1660; υ(C=C) = 1520; υ(C-N) = 1469.

The synthesis of ligands **L_2-L_4** were performed in a similar manner as described for ligand **L_1** using the appropriate carboxylic acids and carboxamides.

1.2. N-(quinolin-8-yl)pyrazine-2-carboxamide (L_2)

Pyrazine-2-carboxylic acid (0.62 g, 5.00 mmol) and 8-aminoquinoline (0.72 g, 5.00 mmol). Light brown solid: Yield: 0.92 g (74%). ^{1}H NMR (400 MHz, DMSO-d_6): δ_H (ppm): 7.67-7.71 (m, 2H, quinoline); 7.77 (dd, $^3J_{HH}$ = 7.8, 1H, quinoline); 8.48 (dd, $^3J_{HH}$ =8.3, 1H, quinoline); 8.86 (dd, $^3J_{HH}$ = 7.6, 1H, quinoline); 8.93 (t, $^3J_{HH}$ = 3.8, 1H, quinoline); 9.01-9.02 (m, 2H, pyrazine); 9.42 (d, $^3J_{HH}$ =1.4, 1H, pyrazine); 11.94 (s, 1H, NH). ^{13}C NMR (DMSO-d6): δC (ppm): 116.06 (CH, quinoline); 122.42 (CH, quinoline); 122.73 (CH, quinoline); 127.02 (CH, quinoline); 127.85 (CH, quinoline); 133.33 (CH, quinoline); 136.73 (C, quinoline); 138.09 (C, quinoline); 143.52 (C, quinoline); 143.73 (CH, pyrazine); 144.06 (CH, pyrazine); 148.22 (CH, pyrazine); 149.37 (C, pyrazine); 160.76 (C=O). FT-IR (cm^{-1}): υ(N-H) = 3303; υ(C=O) =1674; υ(C=C) = 1530; υ(amidic C-N) = 1482.

1.3. N-(quinolin-8-yl)picolinamide (L_3)

Pyridine-2-carboxylic acid (0.62 g, 5.00 mmoles) and 8-aminoquinoline (0.72 g, 5.00 mmoles). Light brown solid. Yield: 0.90 g (72%).^{1}H NMR (400 MHz, DMSO-d_6): δ_H (ppm): 7.67-7.72 (m,

2H, quinoline); 7.73- 7.78 (m, 2H, quinoline); 8.14 (t, $^3J_{HH}$ = 7.8, 1H, quinoline); 8.29 (d, $^3J_{HH}$ = 7.8, 1H, quinoline); 8.48 (d, $^3J_{HH}$ = 8.3, 1H, pyridine); 8.86-8.88 (m, 1H, pyridine); 8.93 (dd, $^3J_{HH}$ = 7.6, 1H, pyridine); 9.04 (dd, $^3J_{HH}$ = 5.9, 1H, pyridine); 12.17 (s, 1H, NH). ^{13}C NMR (DMSO-d6): δC (ppm): 115.86 (CH, quinoline); 122.17 (CH, quinoline); 122.33 (CH, quinoline); 127.04 (CH, quinoline); 127.24 (CH, quinoline); 127.88 (CH, quinoline); 133.71 (C, quinoline); 136.66 (C, quinoline); 138.21 (C, quinoline); 138.37 (CH, pyridine); 148.81 (CH, pyridine); 149.29 (CH, pyridine), 149.36 (C, pyridine), 161.84 (C=O). FT-IR (cm^{-1}): υ(N-H) = 3290; υ(C=O) =1672; υ(C=C) = 1518; υ(amidic C-N) = 1480.

1.4. N-(quinolin-8-yl)quinoline-2-carboxamide (L_4)

Quinoline-2-carboxylic acid (0.86 g, 5.00 mmol) and 8-aminoquinoline (0.72 g, 5.00 mmoles). Light brown solid. Yield: 1.12 g (75%). ^{1}H NMR (400 MHz, DMSO-d_6): δ_H (ppm): 7.70-7.76 (m, 2H, quinoline); 7.78-7.84 (m, 2H, quinoline); 7.98 (t, $^3J_{HH}$ = 7.6, 1H, quinoline); 8.18 (d, $^3J_{HH}$ = 8.1, 1H, quinoline); 8.30 (d, $^3J_{HH}$ = 8.5, 1H, quinoline); 8.39 (d, $^3J_{HH}$ = 8.5, 1H, quinoline); 8.50 (dd, $^3J_{HH}$ = 8.3, 1H, quinoline); 8.73 (d, $^3J_{HH}$ = 8.5, 1H, quinoline); 8.96 (dd, $^3J_{HH}$ = 7.6, 1H, quinoline); 9.11(dd, $^3J_{HH}$ = 5.9, 1H, quinoline); 12.39 (s, 1H, NH). ^{13}C NMR (DMSO-d6): δC (ppm): 115.89; 118.49; 122.43; 127.09; 127.94; 128.21; 128.57; 129.15; 129.36; 130.94, 133.76; 136.69; 138.36; 138.62; 145.80; 149.45; 149.59 (quinoline carbons); 161.95 (C=O). FT-IR (cm^{-1}): υ(N-H) = 3300; υ(C=O) =1680; υ(C=C) = 1545; υ(amidic C-N) = 1492.

2. ^{1}H NMR spectra of ligands

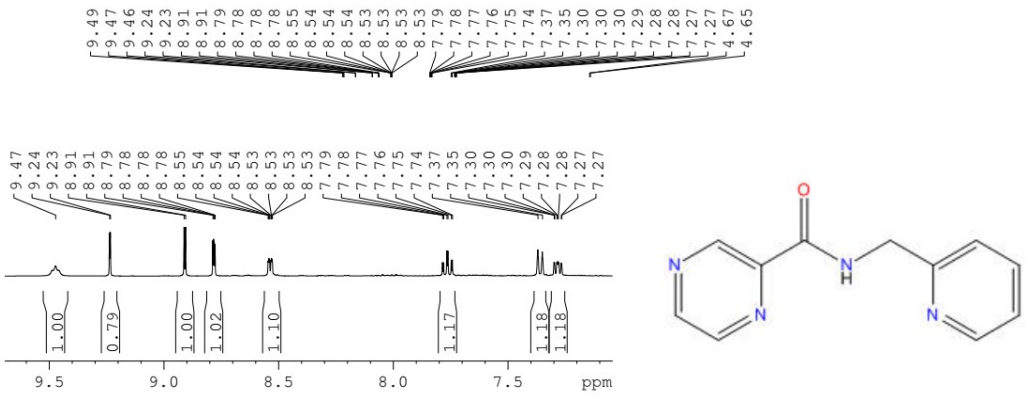

Fig. S1: ^{1}H NMR of $\mathbf{L_1}$

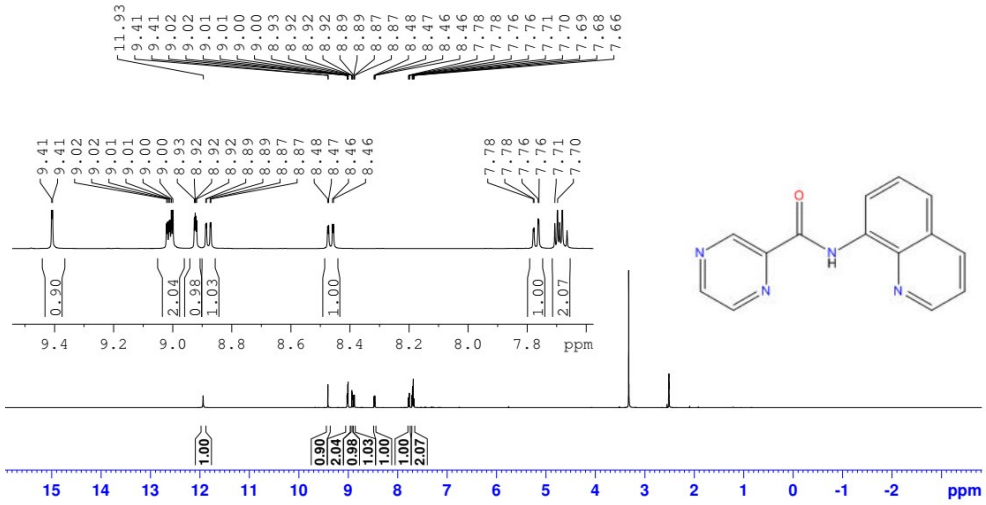

Fig. S2: ^{1}H NMR of $\mathbf{L_2}$

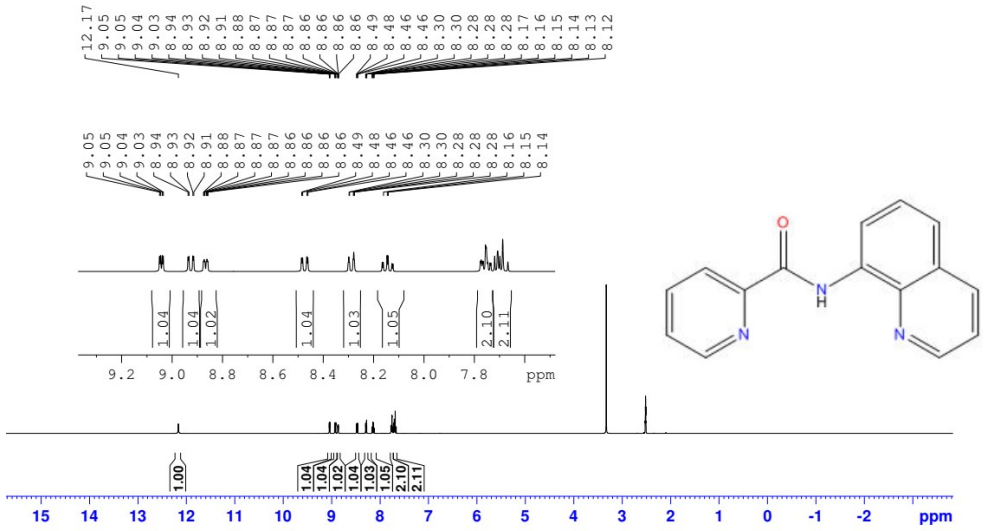

Fig. S3: ^{1}H NMR of $\mathbf{L_3}$

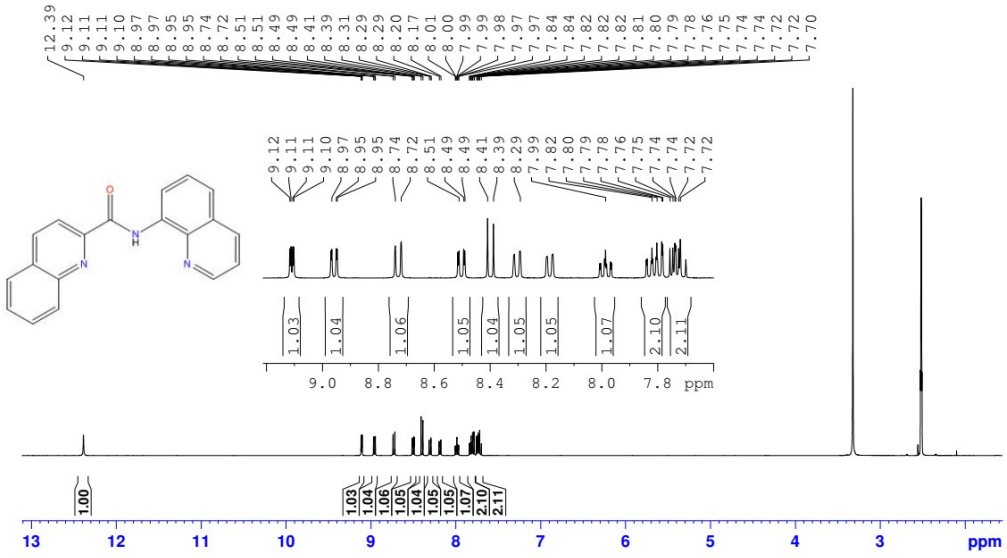

Fig. S4: ^{1}H NMR of $\mathbf{L_4}$

3. ^{1}H NMR spectra of Pd(II) complexes

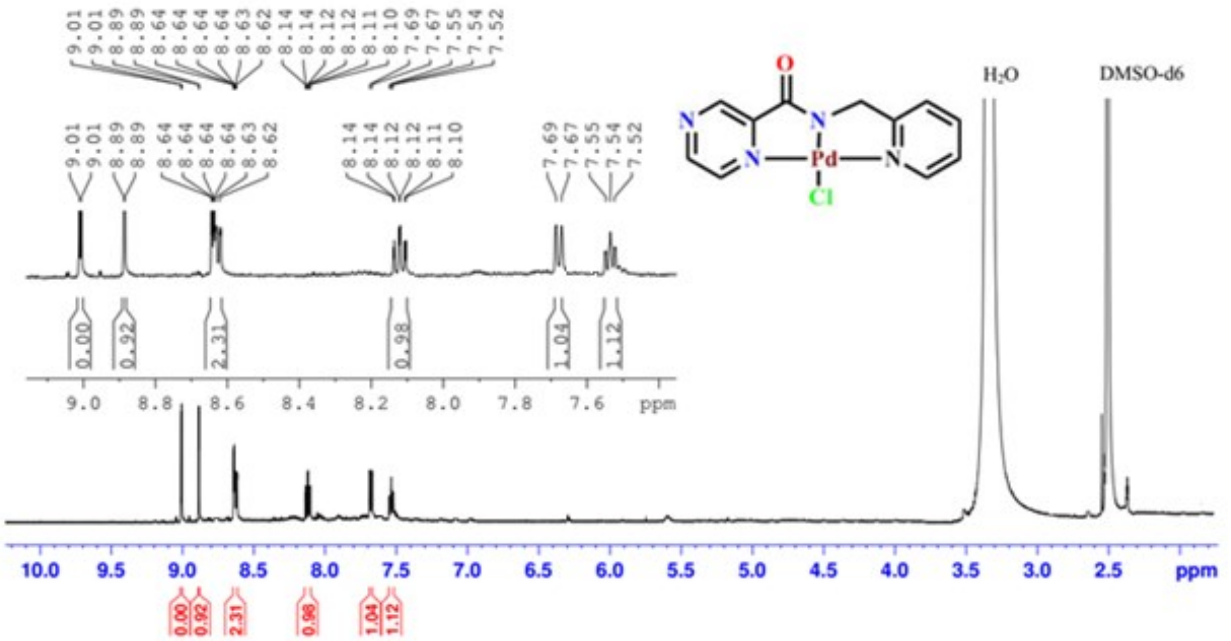

Fig. S5: ^{1}H NMR of **PdL_1**

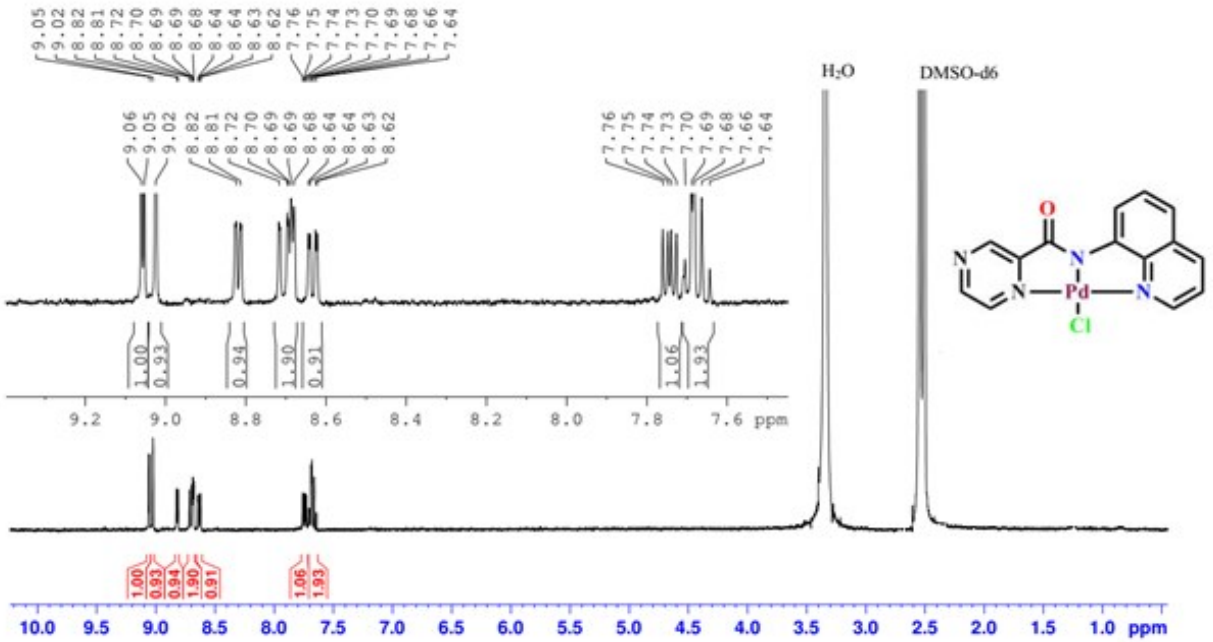

Fig. S6: ^{1}H NMR of **PdL_2**

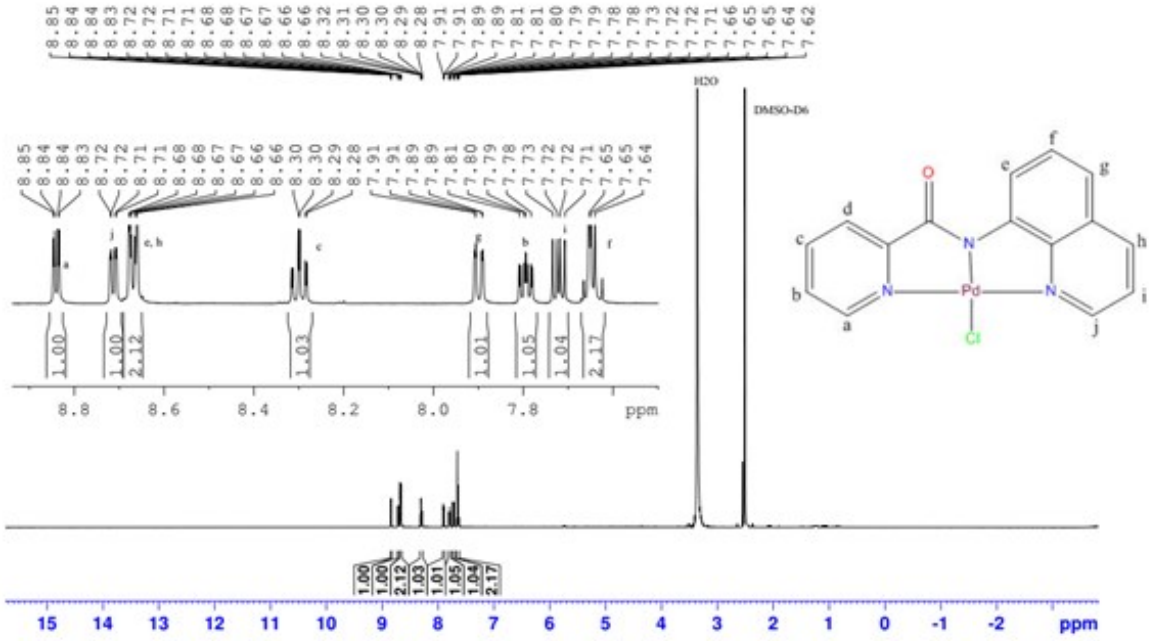

Fig. S7: ^{1}H NMR of **PdL$_3$**

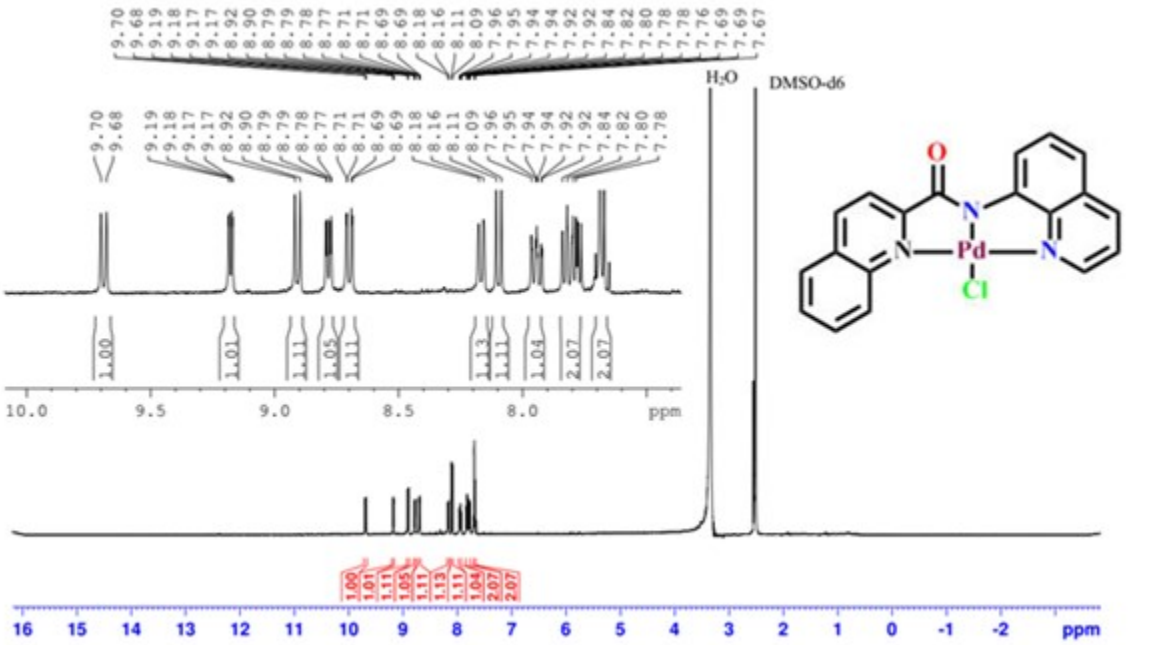

Fig. S8: ^{1}H NMR of **PdL$_4$**

4. ^{13}C NMR spectra of ligands

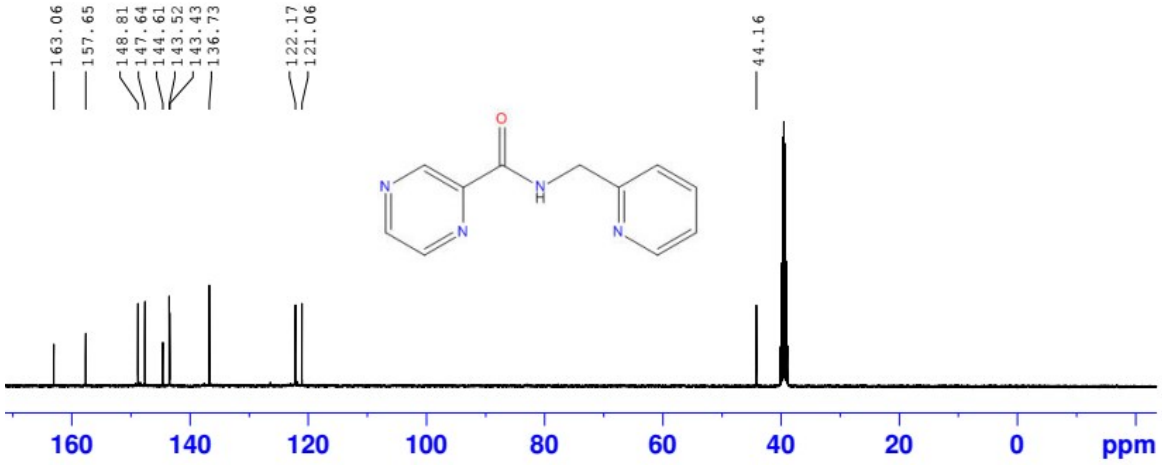

Fig. S9: ^{13}C NMR of $\mathbf{L_1}$

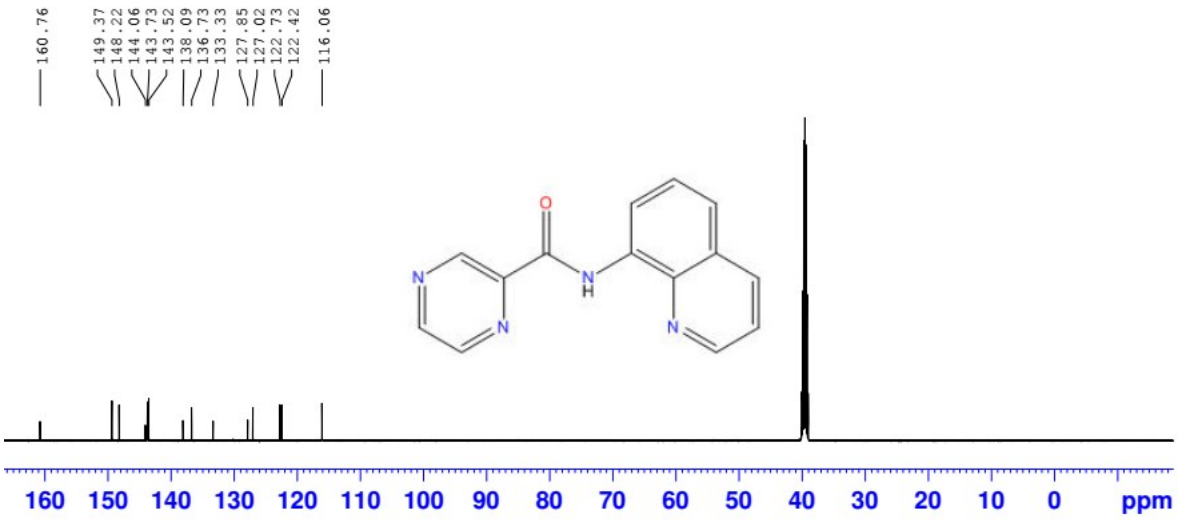

Fig. S10: ^{13}C NMR of $\mathbf{L_2}$

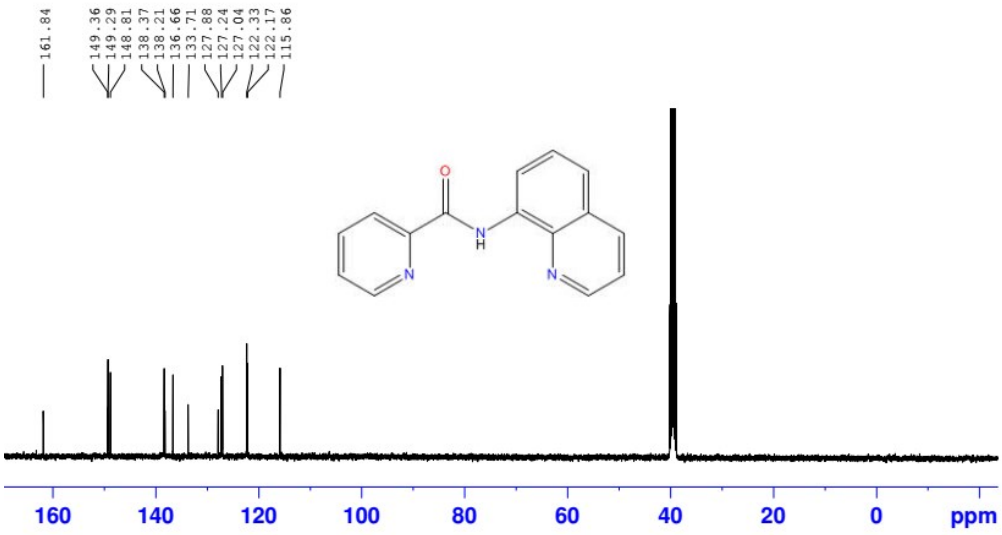

Fig. S11: ^{13}C NMR of $\mathbf{L_3}$

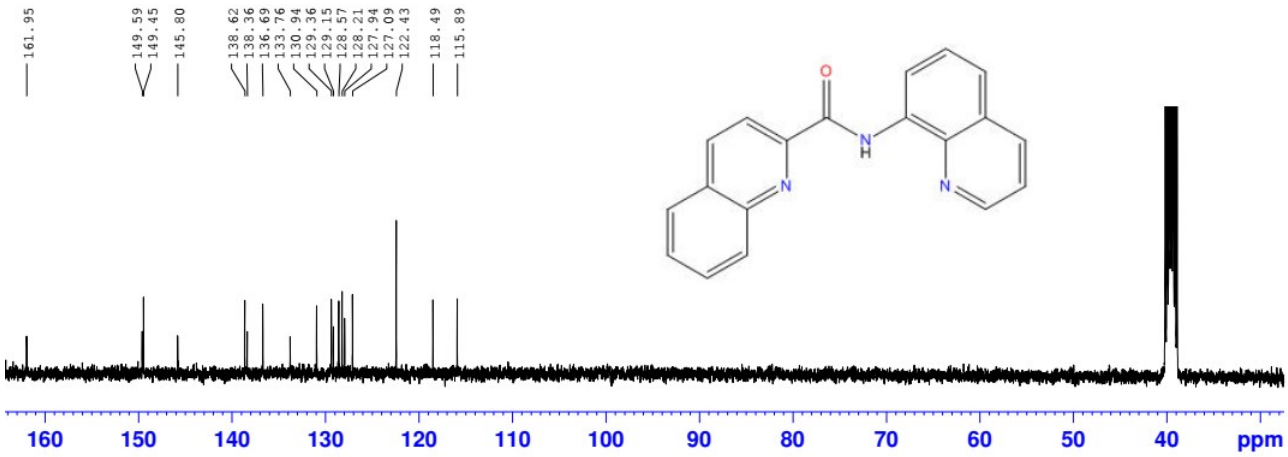

Fig. S12: ^{13}C NMR of $\mathbf{L_4}$

5. ^{13}C NMR spectra of Pd(II) complexes

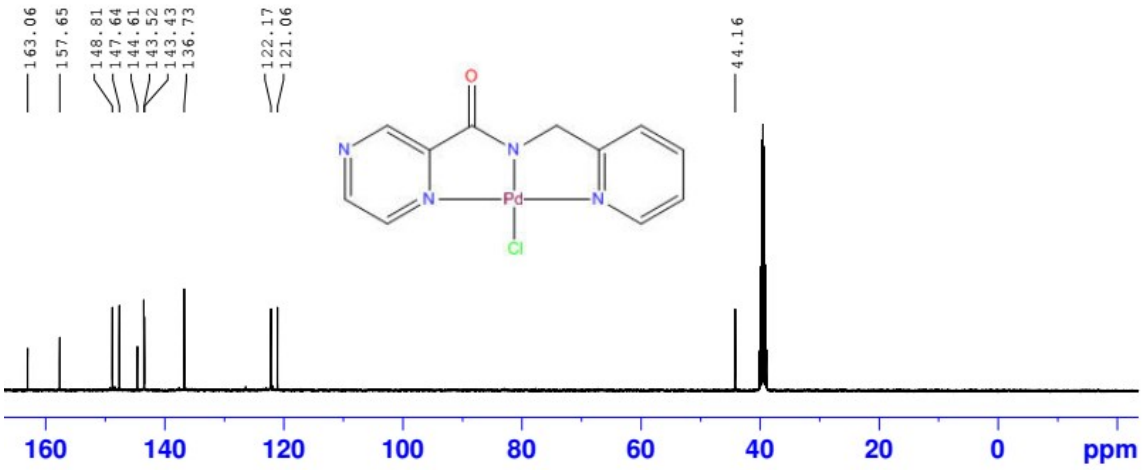

Fig. S13: ^{13}C NMR of **PdL_1**.

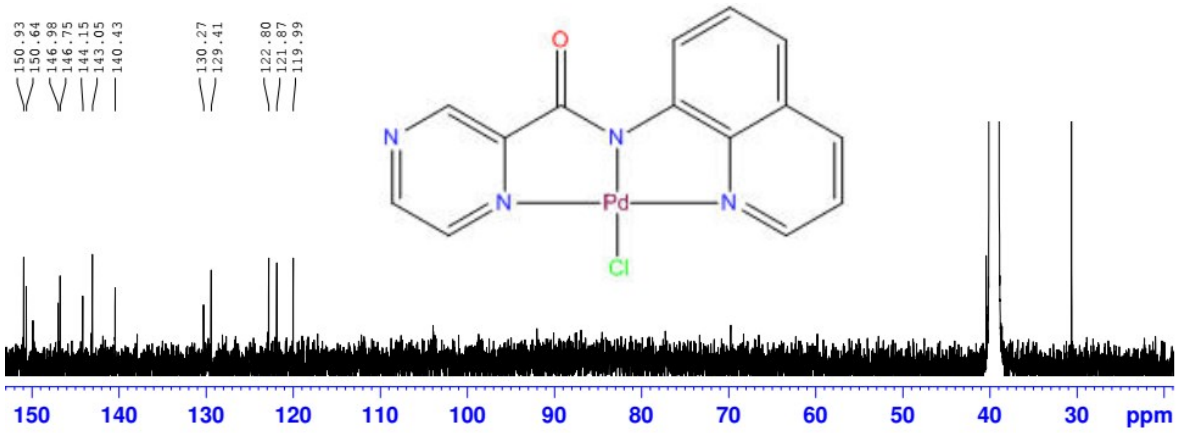

Fig. S14: ^{13}C NMR of **PdL_2**

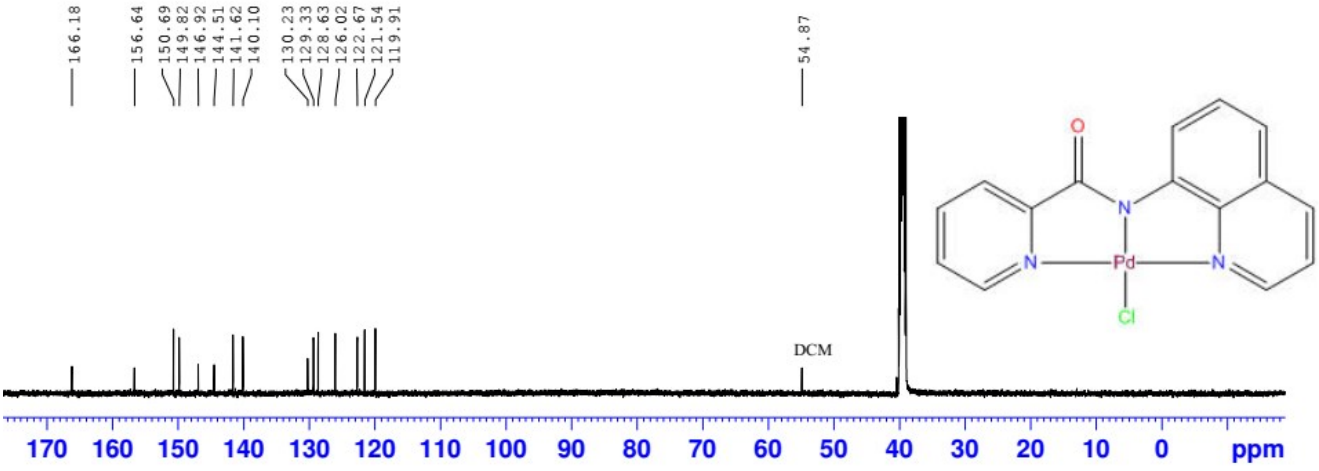

Fig. S15: ^{13}C NMR of **PdL_3**

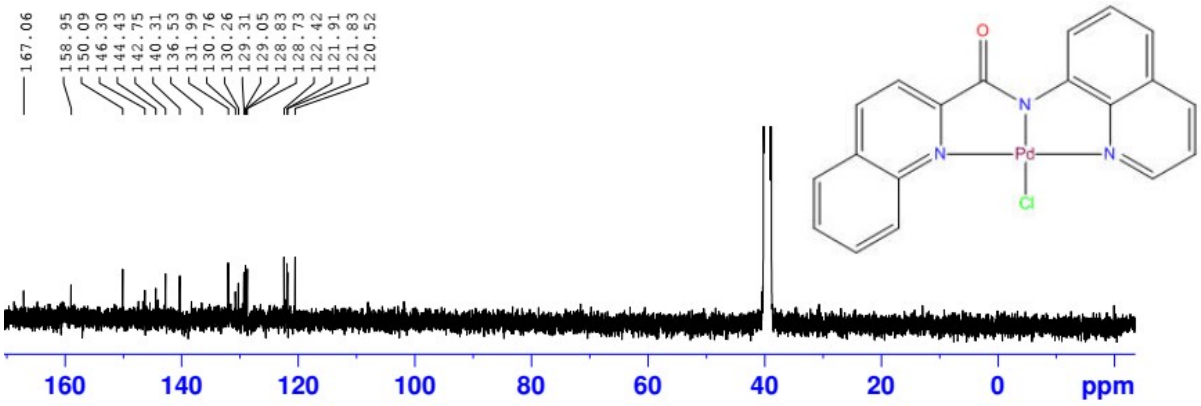

Fig. S16: ^{13}C NMR of **PdL_4**

6. FT-IR spectra of the ligands and their respective Pd-complexes

6.1 FT-IR for ligands

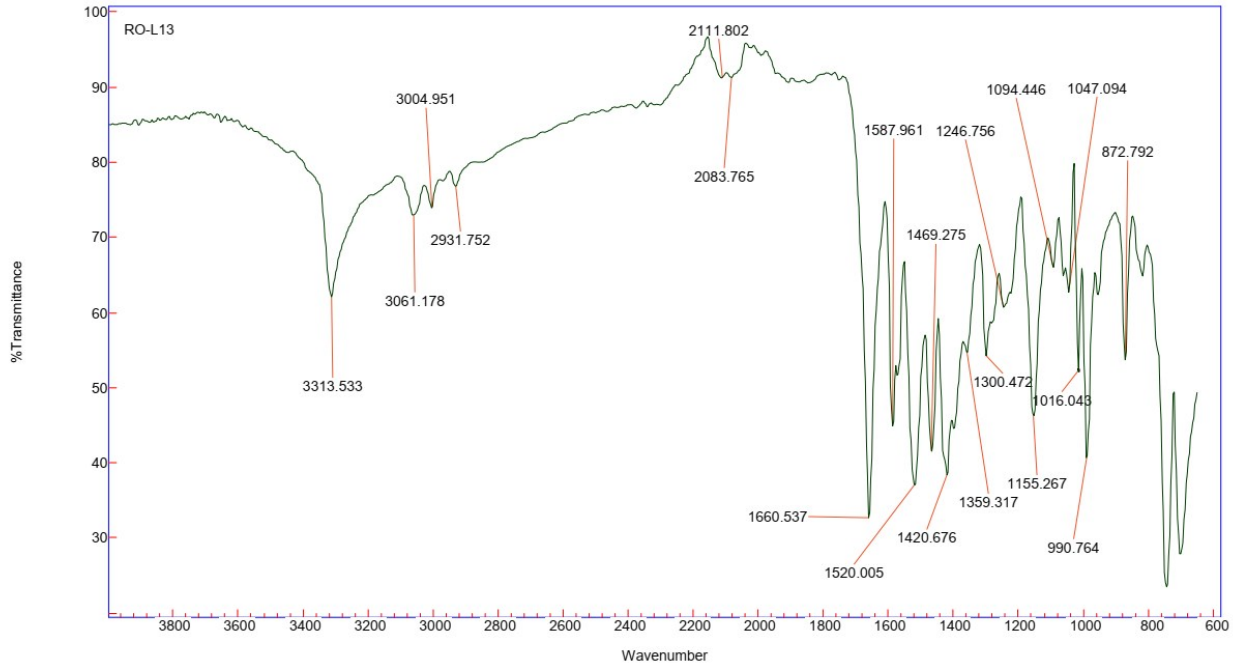

Fig. S17: FT-IR of $\mathbf{L_1}$

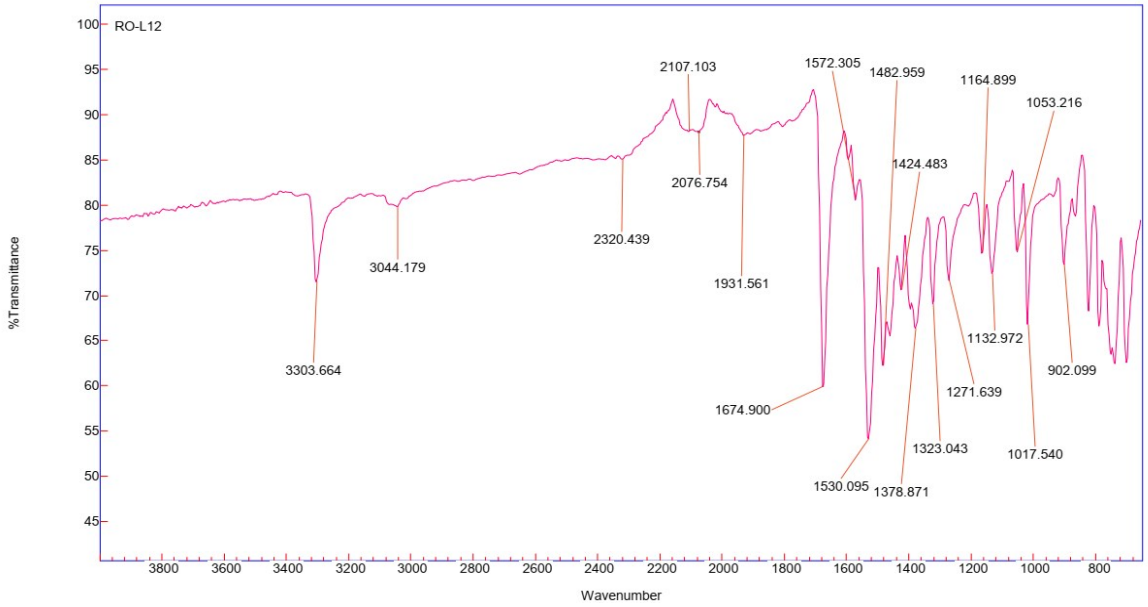

Fig. S18: FT-IR of $\mathbf{L_2}$

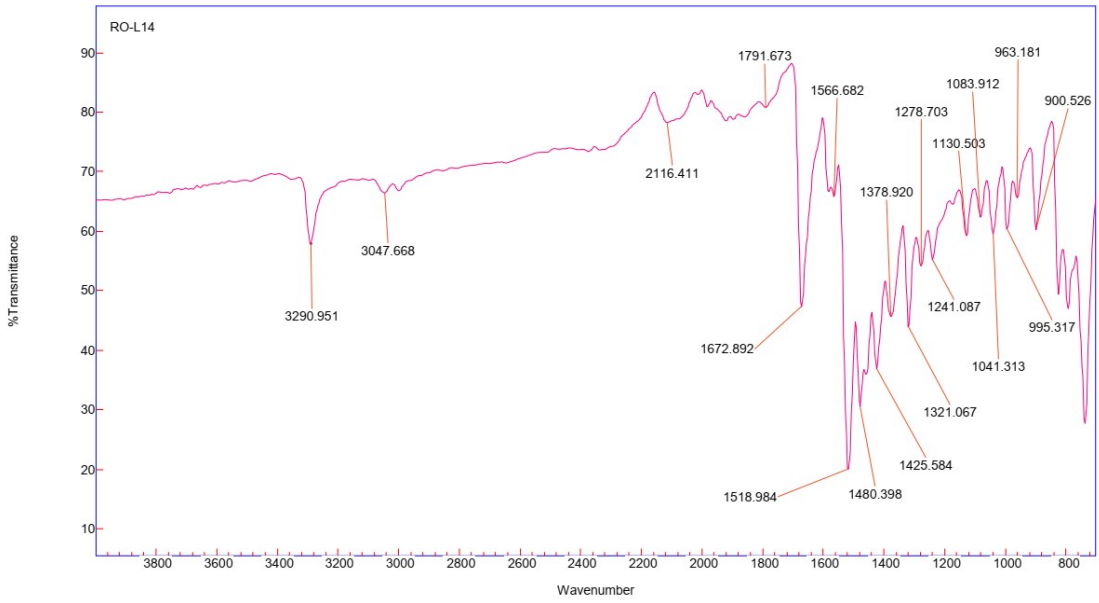

Fig. S19: FT-IR of $\mathbf{L_3}$

6.2 FT-IR for Pd(II) complexes

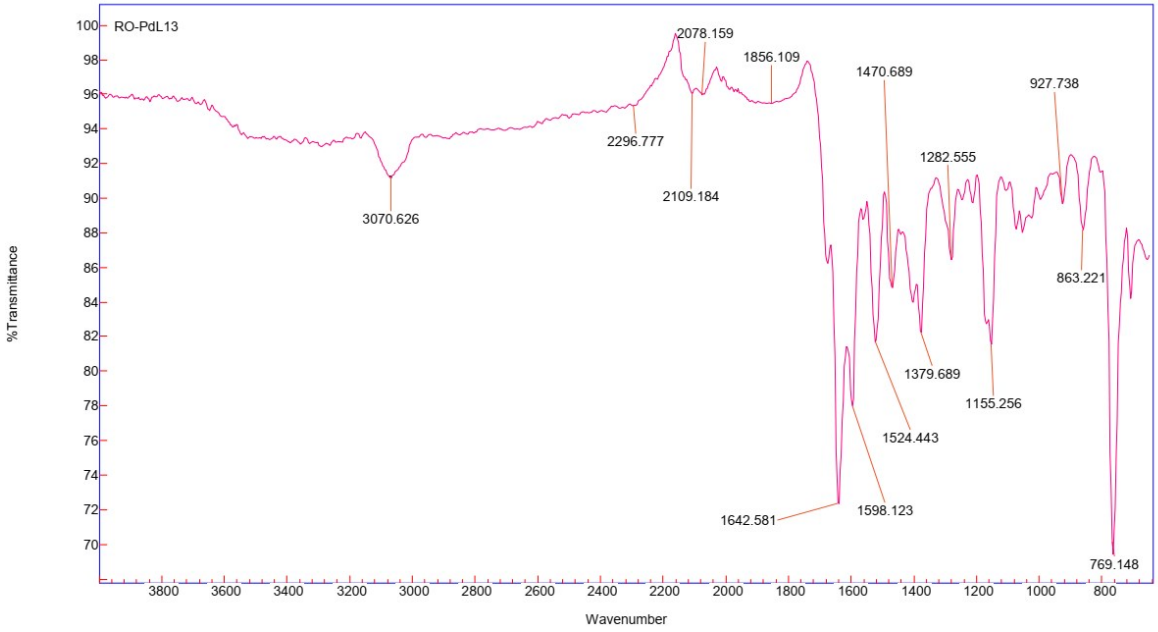

Fig. S20: FT-IR of $\mathbf{PdL_1}$

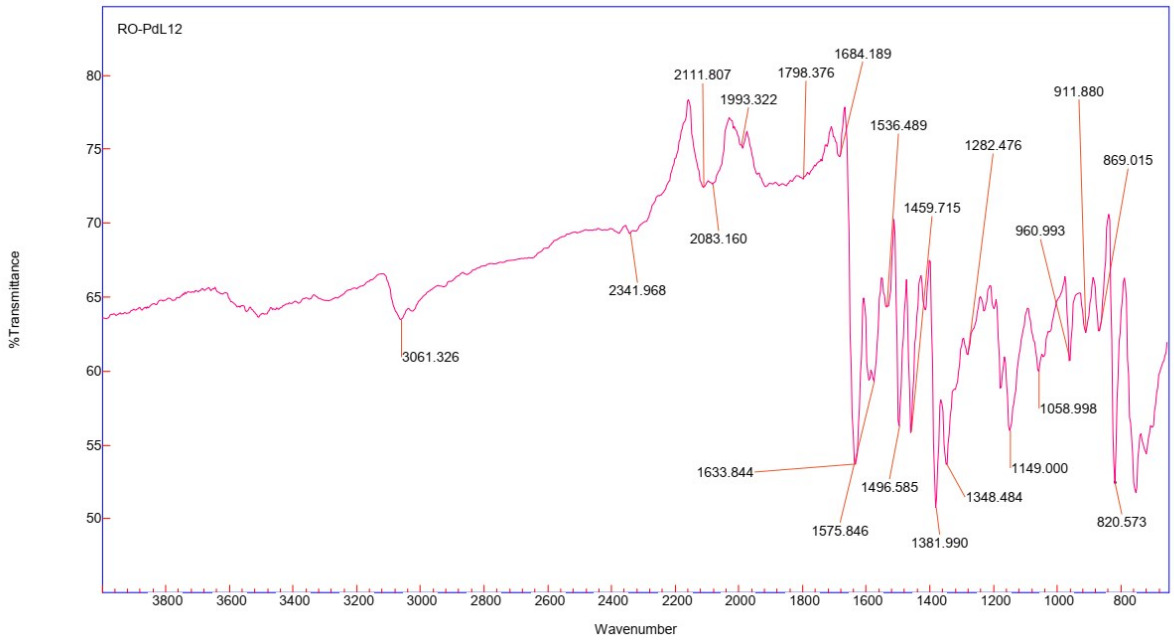

Fig. S21: FT-IR of **PdL_2**

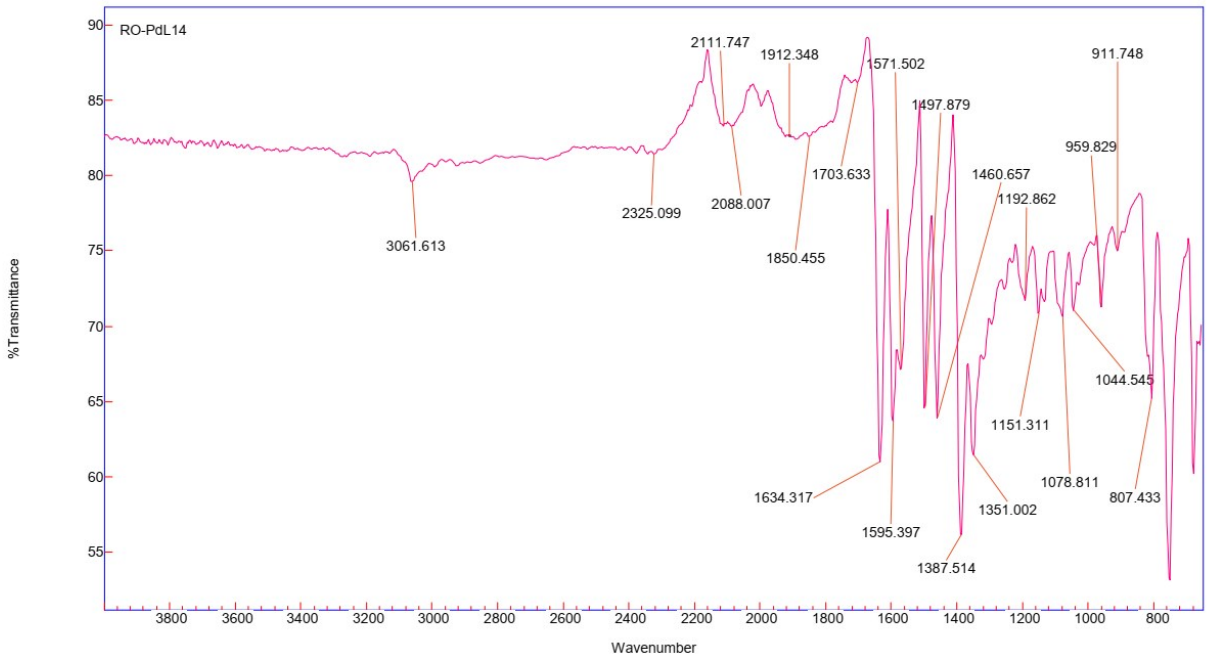

Fig. S22: FT-IR of **PdL_3**

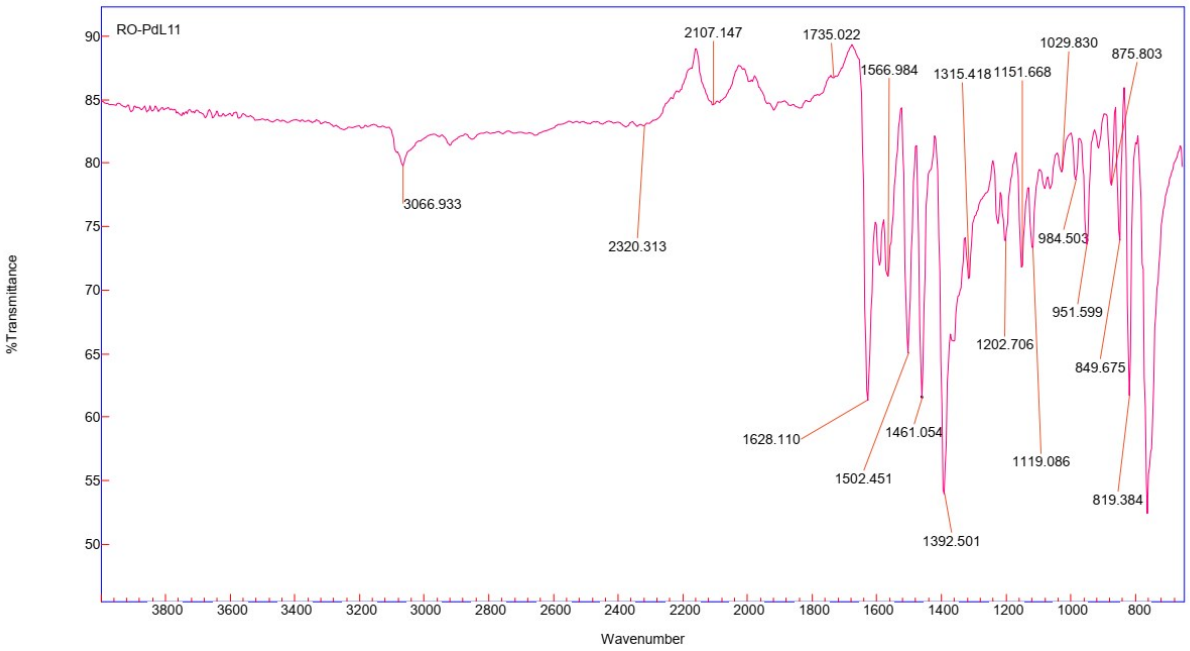

Fig. S23: FT-IR of **PdL_4**

8. DFT details for the complexes

Geometry optimised structure	HOMO map	LUMO map	Planarity
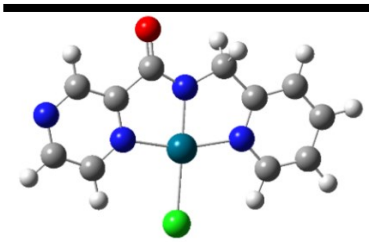 **PdL_1**	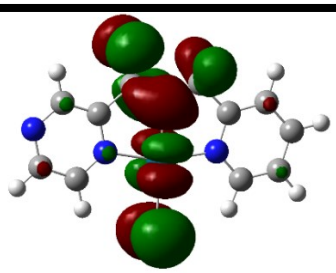	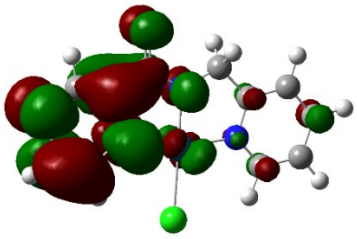	
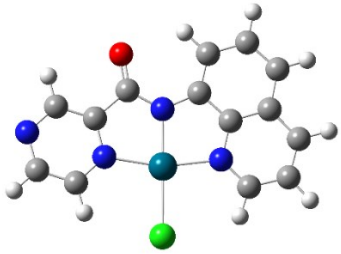 **PdL_2**	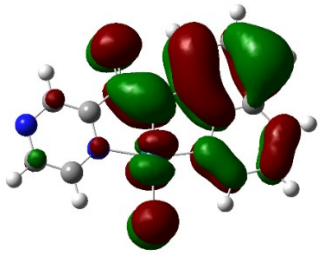	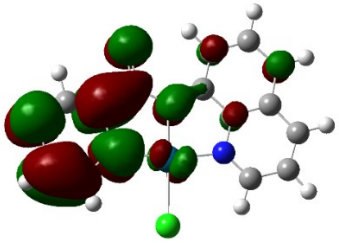	
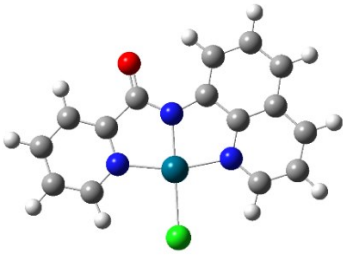 **PdL_3**	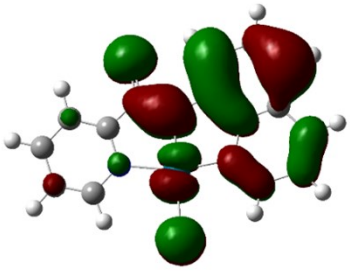	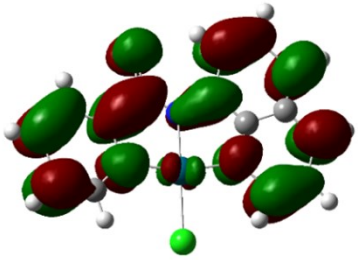	
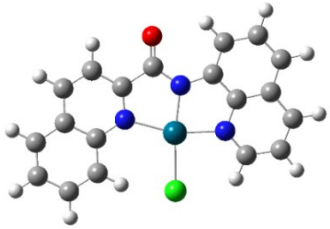 **PdL_4**	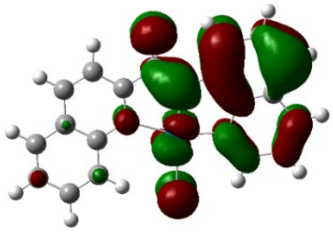	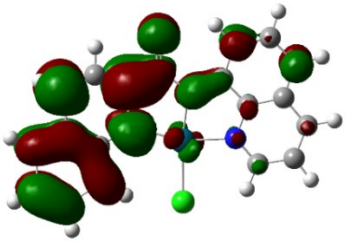	

Fig. S24: DFT-optimised HOMO, LUMO frontier molecular orbitals, with respective planarity structures of **PdL_1-PdL_4**.

9. Electrochemical voltammograms for the complexes

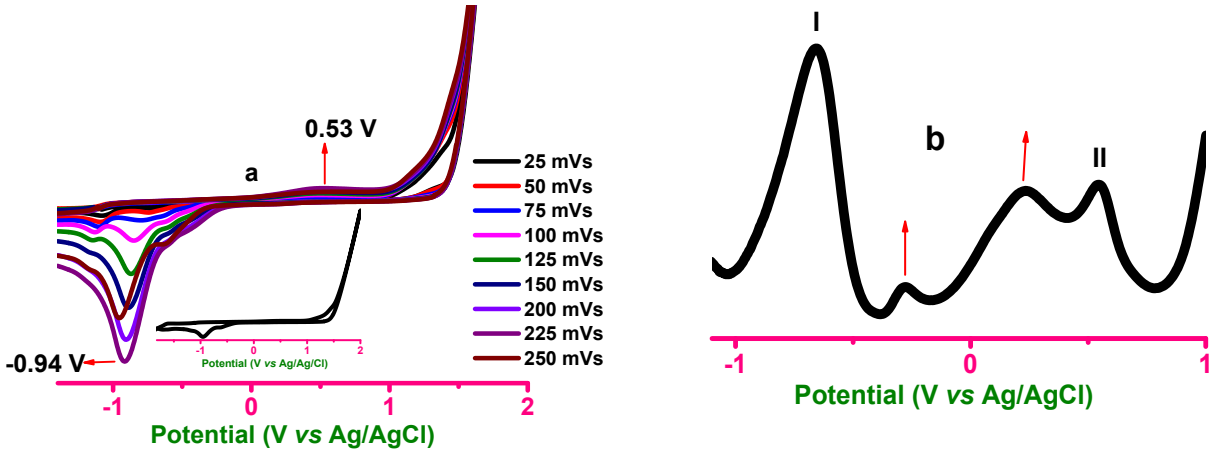

Fig. S25: (a); Overlays of CV; (b) SWV of **PdL$_1$** in DMSO. The arrows denote aggregate peaks.

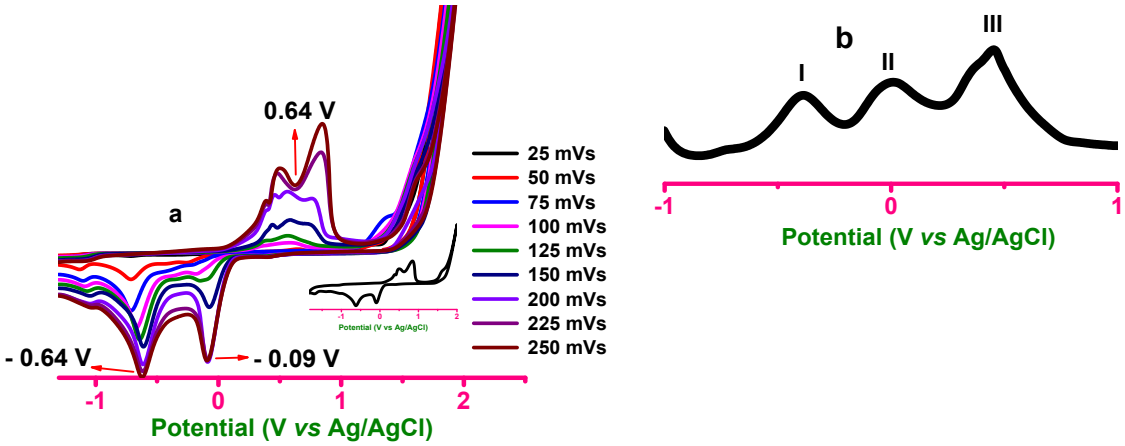

Fig. S26: (a); Overlays of CV; (b) SWV of **PdL$_3$** in DMSO. The arrows denote aggregate peaks.

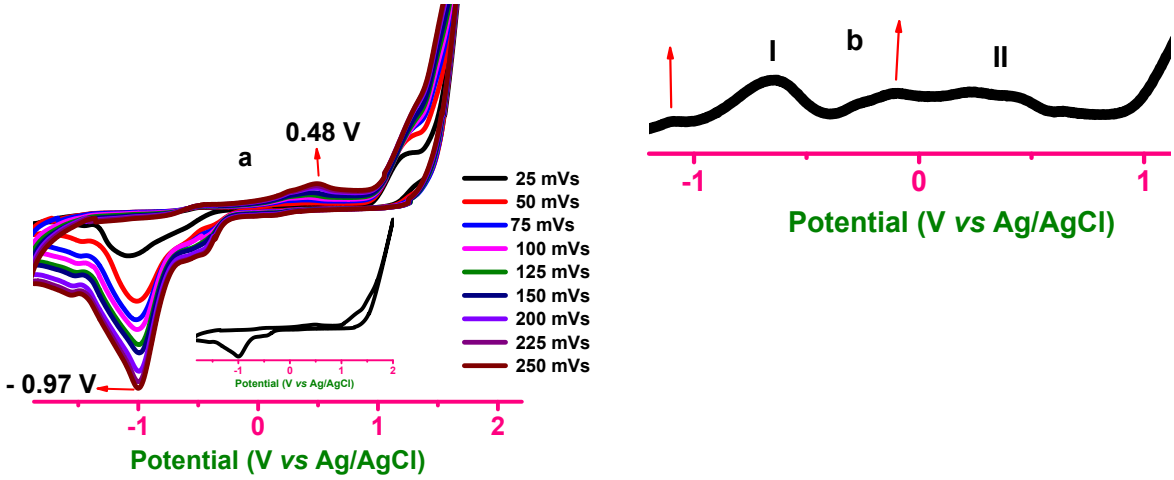

Fig. S27: Overlays of CV; (b) SWV of **PdL_4** in DMSO. The arrows denote aggregate peaks.

10. Stability of complexes in aqueous and DMSO solutions

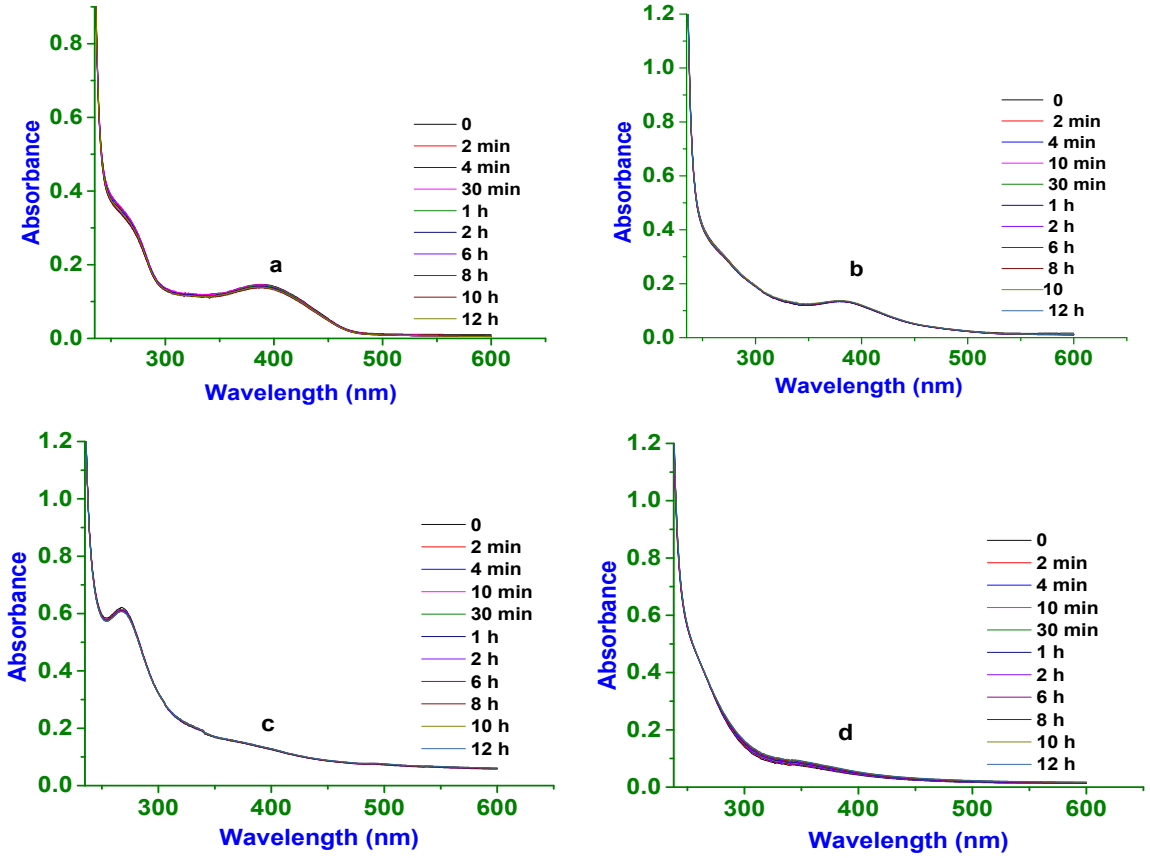

Fig. S28: UV–Vis spectra of **PdL_1** (a), **PdL_2** (b), **PdL_3** (c), and **PdL_4** (d) in buffer (pH = 7.4) over a 12 h period.

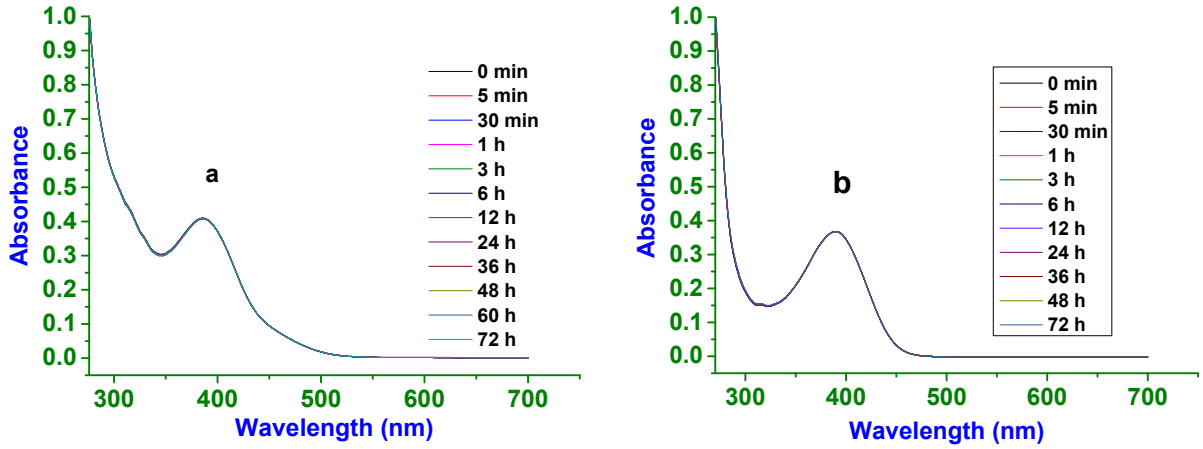

Fig. S29: UV-Vis absorption spectra of **PdL_2** (a), **PdL_3** (b) in DMSO over a 72 h period.

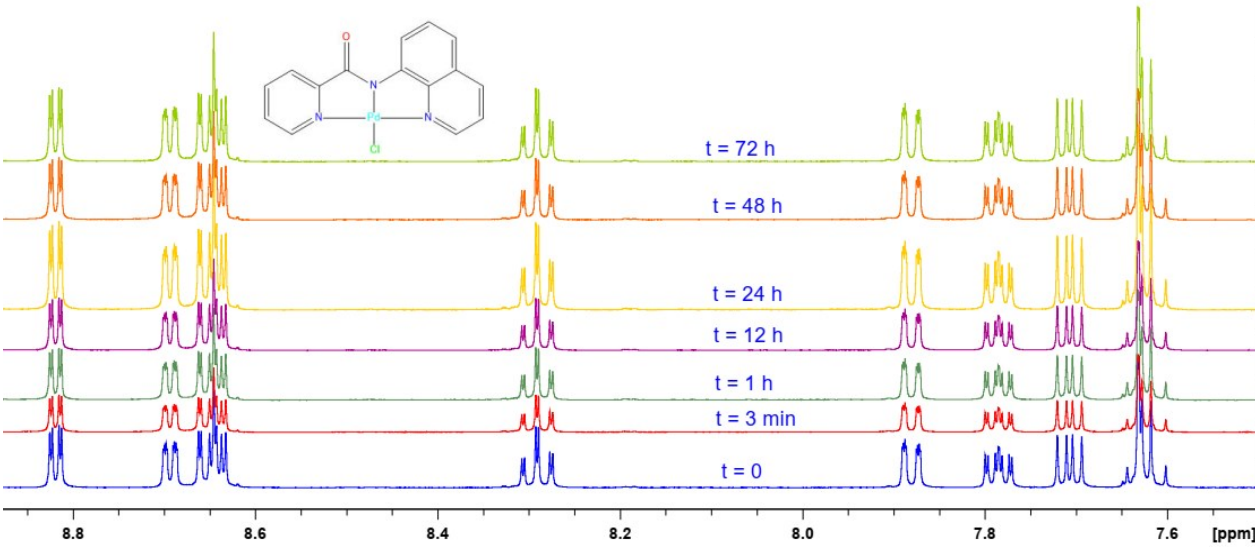

Fig. S30: ^{1}H NMR spectral data of **PdL_4** in DMSO-d6 over 72 h.

11. Dependence of k_{obs} on the nucleophile concentration

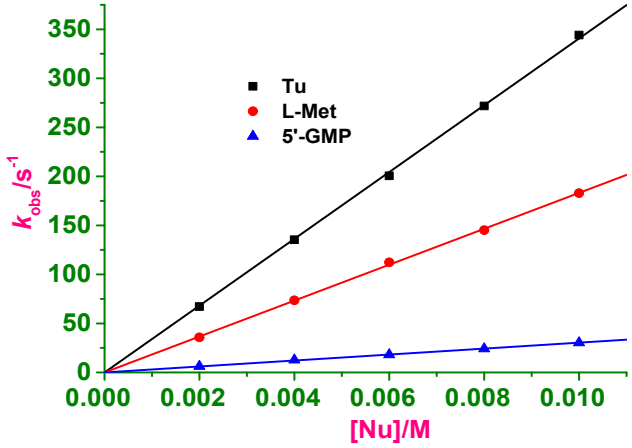

Fig. S31: Dependence of k_{obs} on [Nu] for **PdL_2**

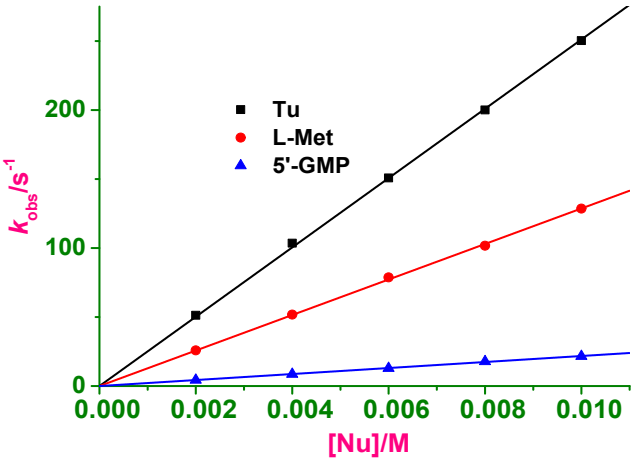

Fig. S32: Dependence of k_{obs} on [Nu] for **PdL_3**

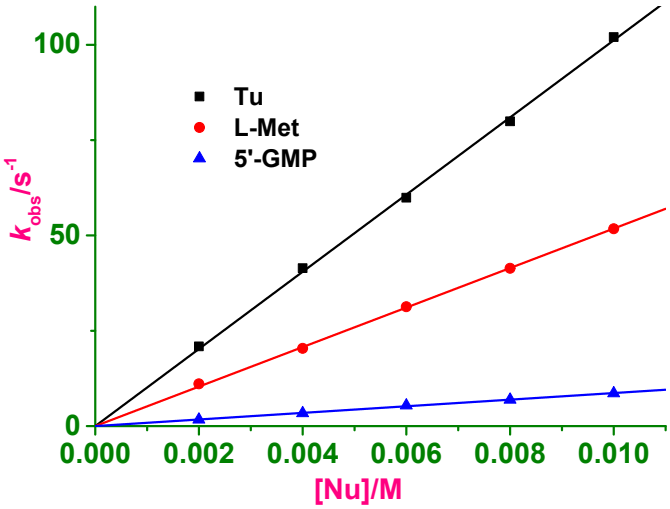

Fig. S33: Dependence of k_{obs} on [Nu] for **PdL$_4$**

12. Eyring plots for the reaction of complexes with the nucleophiles

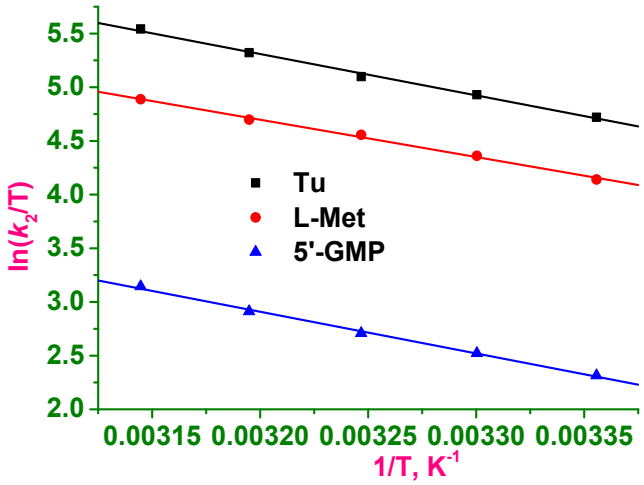

Fig. S34: Eyring plots for **PdL$_2$**

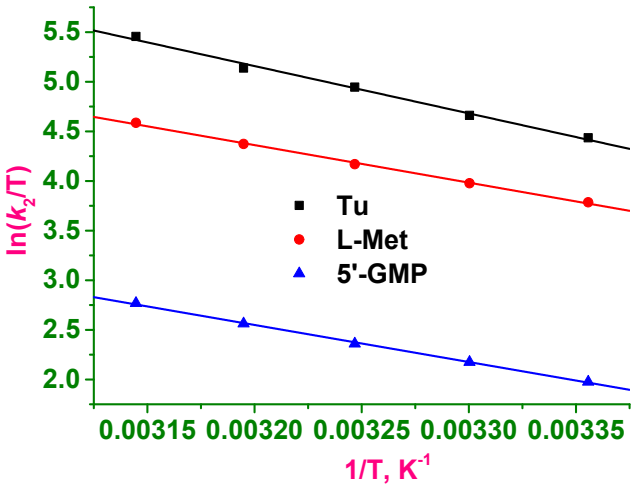

Fig. S35: Eyring plots for **PdL_3** .

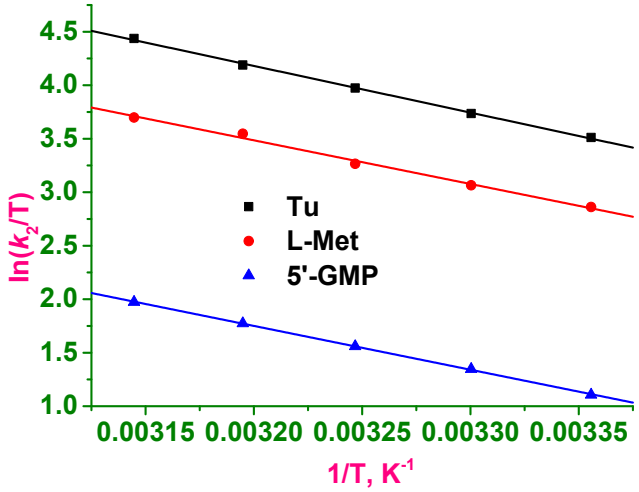

Fig. S36: Eyring plots for **PdL_4**

13. UV-visible absorption measurements for CT-DNA studies

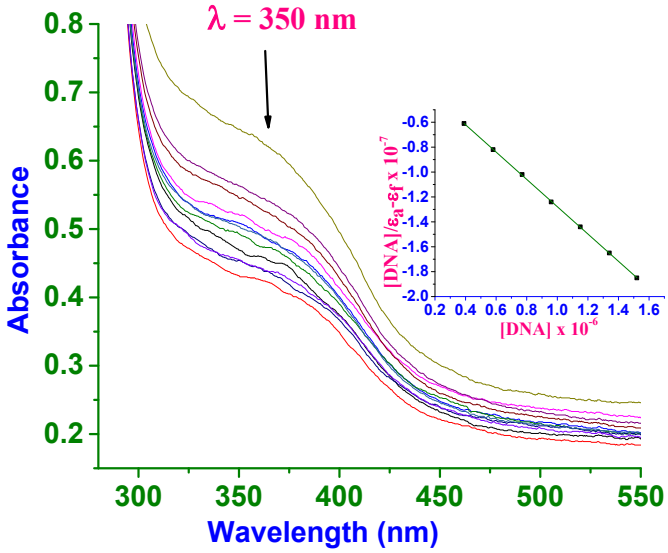

Fig. S37: Absorption spectra for **PdL_1**

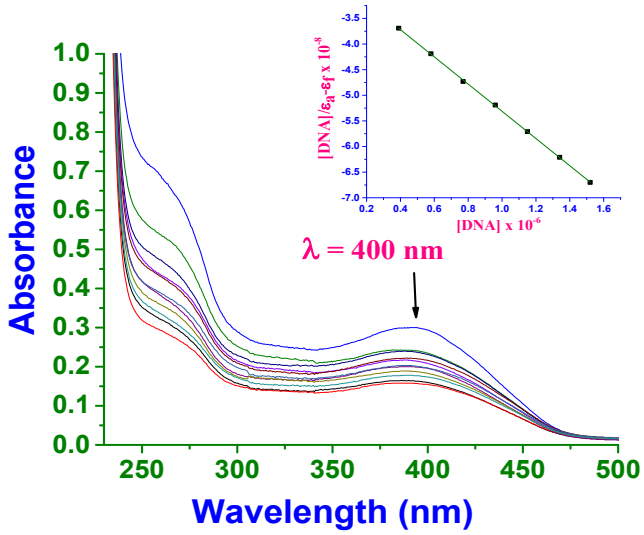

Fig. S38: Absorption spectra for **PdL_2**

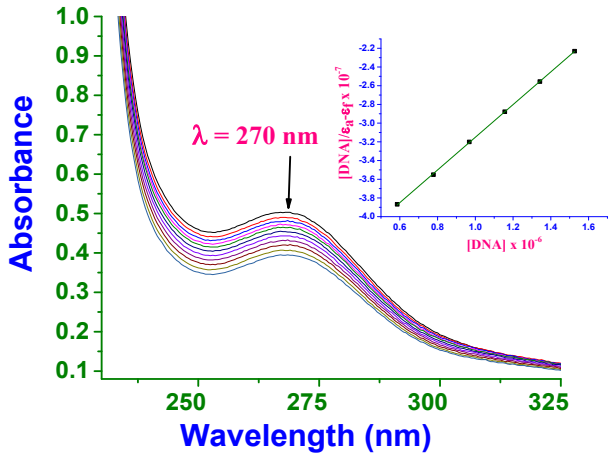

Fig. S39: Absorption spectra for **PdL_3**

14. Fluorescence emission spectra of EB bounded to CT-DNA studies

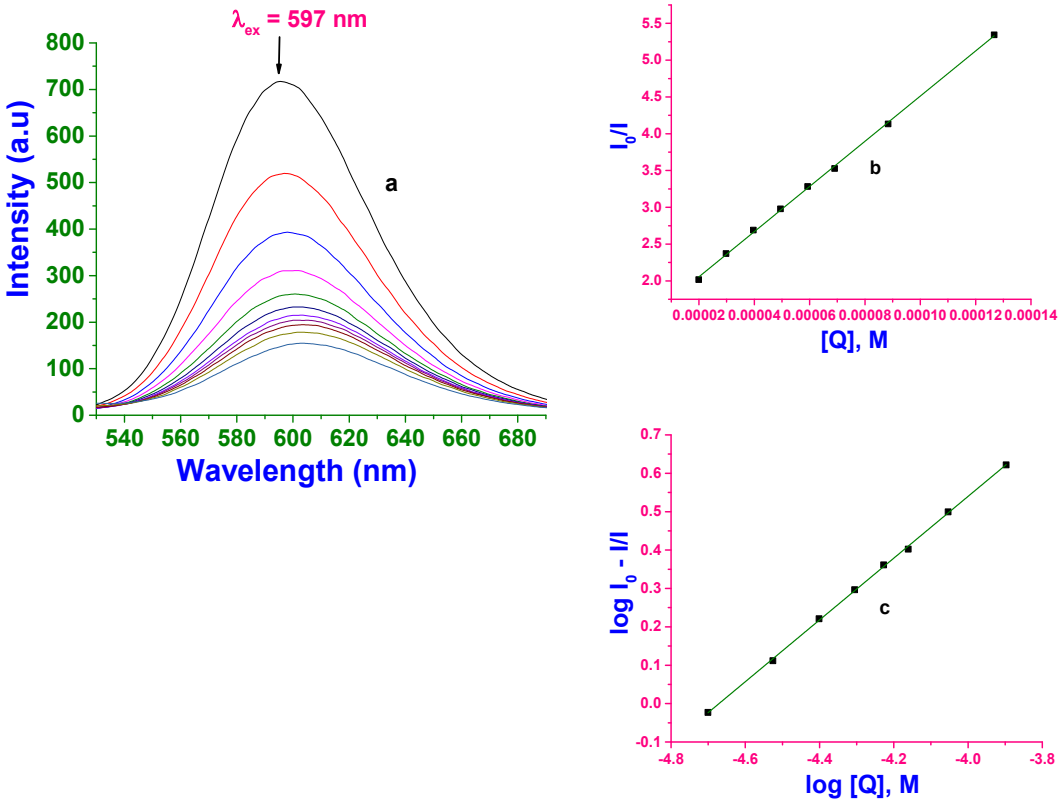

Fig. S40: (**a**); Fluorescence emission of EB-CT-DNA in **PdL_1**: [EB] = 50 µM, [CTDNA] = 50 µM and [**PdL1**] = 0-400 µM. (**b**); Stern-Volmer plot of Io/I vs [Q]. (**c**); Scatchard plot of log[(Io–I)/I] vs log[Q].

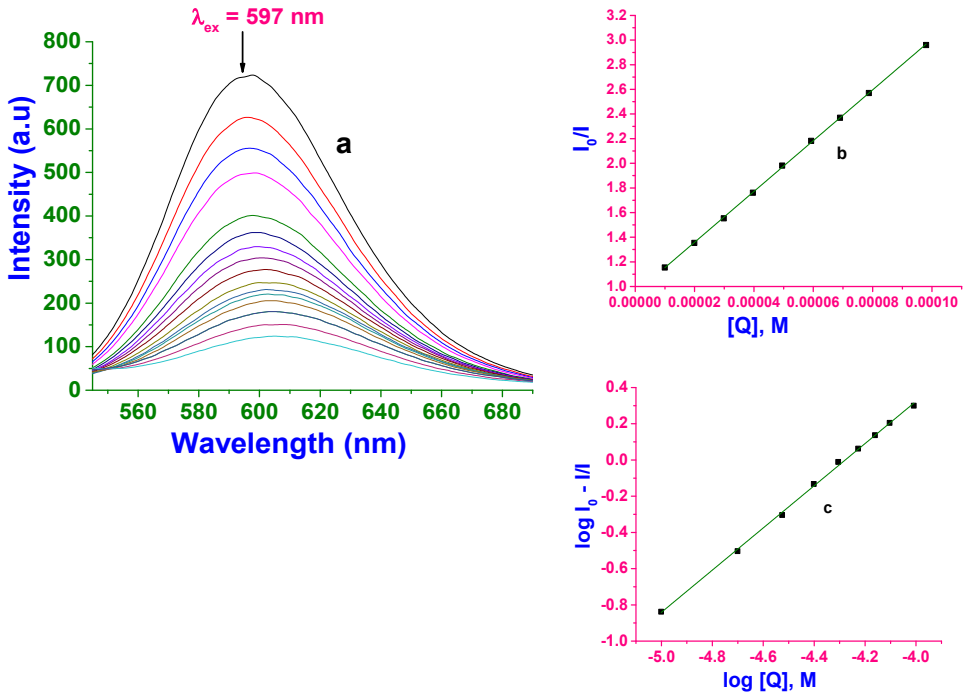

Fig. S41: (**a**); Fluorescence emission of EB-CT-DNA in **PdL$_2$**: [EB] = 50 µM, [CTDNA] = 50 µM and [**PdL$_2$**] = 0 - 400 µM. **(b)**; Stern-Volmer plot of I_o/I *vs* [Q]. **(c)**; Scatchard plot of log[(I_o–I)/*I*] *vs* log[Q].

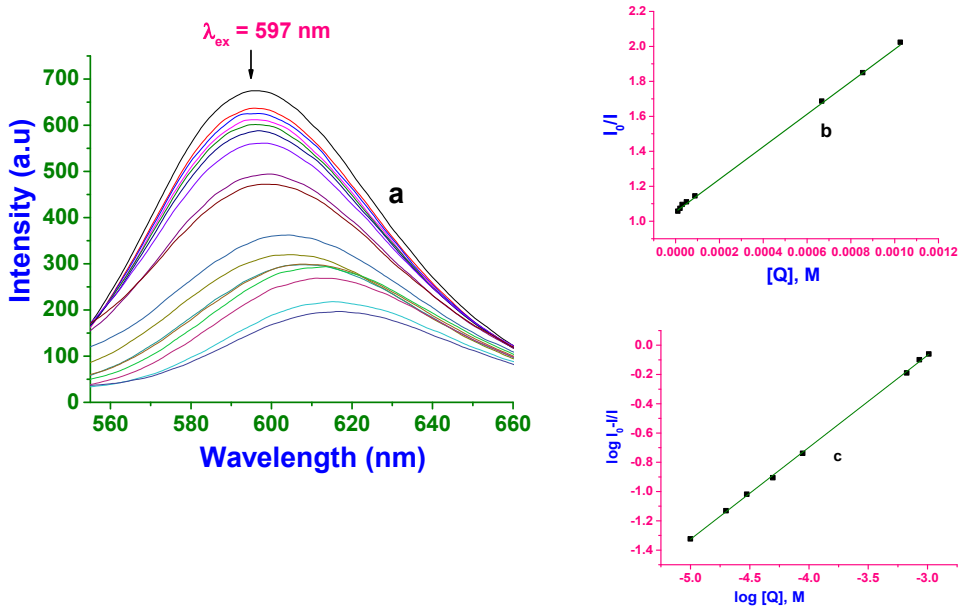

Fig. S42: (**a**); Fluorescence emission of EB -CT-DNA in **PdL$_3$**: [EB] = 50 µM, [CTDNA] = 50 µM and [**PdL$_3$**] = 0-400 µM. (**b**); Stern-Volmer plot of Io/I vs [Q]. (**c**); Scatchard plot of log[(Io–I)/I] vs log[Q].

15. Fluorescence emission spectra of BSA studies

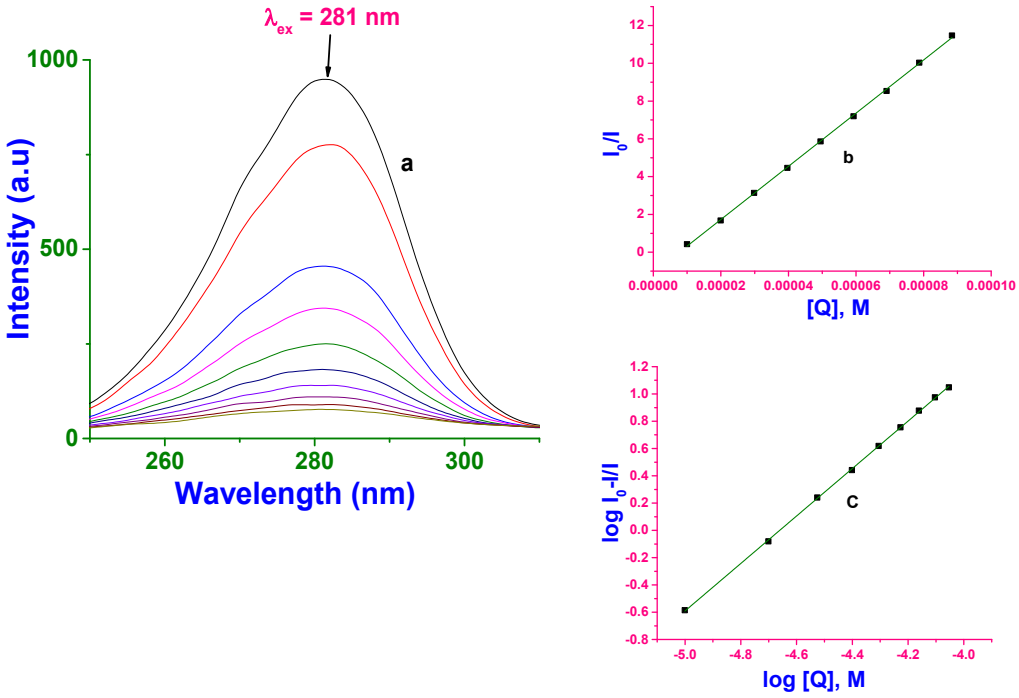

Fig. S43: (a): Fluorescence emission of BSA for $\mathbf{PdL_2}$: [BSA] = 12 μM and [$\mathbf{PdL_2}$] = 0-10 μM. **(b)**: Stern-Volmer plot of I_o/I *vs* [Q] and **(c)**: Scatchard plot of log[$(I_o–I)/I$] *vs* log[Q]

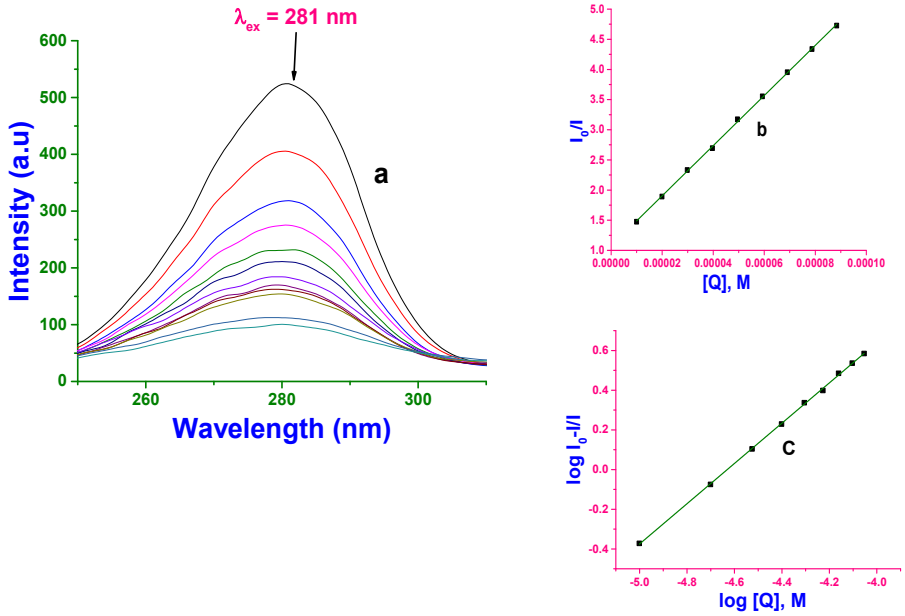

Fig. S44: (**a**); Fluorescence emission of BSA for PdL3: [BSA] = 12 μM and [**PdL$_3$**] = 0-10 μM. (**b**): Stern-Volmer plot of Io/I *vs* [Q] and (**c**): Scatchard plot of log[(Io–I)/I] *vs* log[Q].

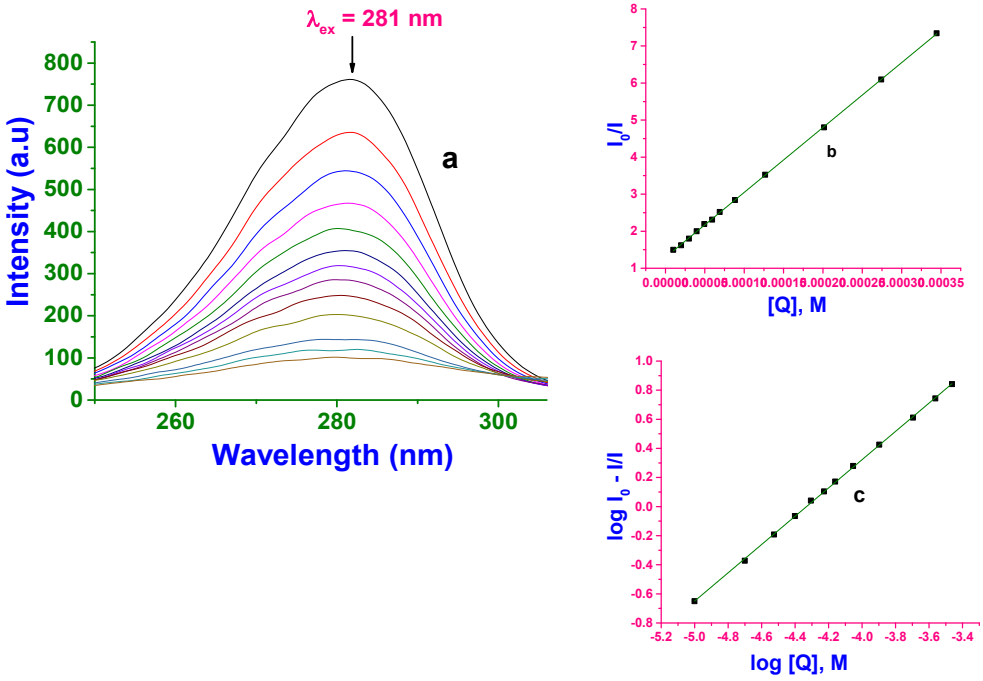

Fig. S45: (**a**); Fluorescence emission of BSA for **PdL$_4$**: [BSA] = 12 μM and [**PdL$_4$**] = 0-10 μM. (**b**): Stern-Volmer plot of I_o/I *vs* [Q] and (**c**): Scatchard plot of log[(I_o–I)/I] *vs* log[Q].

16. *In silico* DNA binding affinity

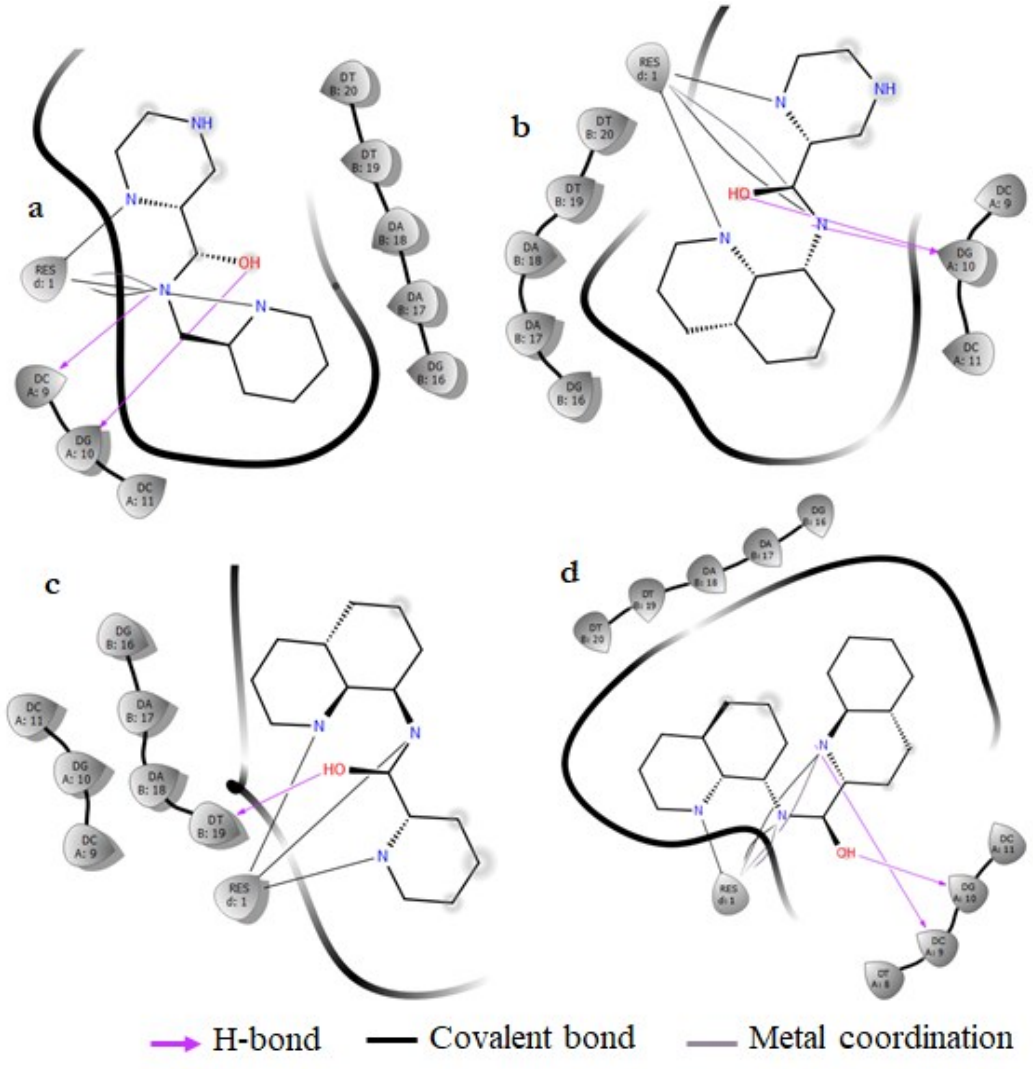

Fig. S46: Interacting atoms and molecules of DNA-complexes and their specific bonds. a) Interaction of **PdL_1** with B-DNA; the compound forms two hydrogen bond (OH group and N atom) with G10 and C9 with at 1.80 Å and 2.44 Å respectively; b) Interaction of **PdL_2** with B-DNA; the compound forms two hydrogen bond (OH group and N atom) with G10 (1.73 Å) and (2.03 Å) respectively; c). Interaction of **PdL_3** with B-DNA, formed a single hydrogen bond between the OH-group of the compound and the B-chain of the DNA at 2.31 Å; d). Interaction of **PdL_4** with B-DNA; this compound establishes two hydrogen bonds (OH group and N atom) with G10 (2.04 Å) and C9 (2.38 Å) respectively. Other interactions observed include hydrophobic interactions between atoms, metal coordination and covalent bonds between the nitrogen atoms of all the compounds and the residue D1 of the receptor at a distance < 2.5 Å.

17. FT-IR summary for ligands and their respective Pd(II) complexes

Table S1: FT-IR data for ligands $\mathbf{L_1}$-$\mathbf{L_4}$ and their respective Pd(II) complexes

Compounds	υ(N-H)	υ(C=O)	υ(C=C)	υ(C-N)
$\mathbf{L_1}$	3313	1660	1520	1469
$\mathbf{PdL_1}$	-	1642	1524	1470
$\mathbf{L_2}$	3303	1674	1530	1482
$\mathbf{PdL_2}$	-	1633	1575	1459
$\mathbf{L_3}$	3290	1672	1518	1480
$\mathbf{PdL_3}$	-	1634	1595	1497
$\mathbf{L_4}$	3300	1680	1545	1492
$\mathbf{PdL_4}$	-	1628	1502	1461

18. Crystal data information for the complexes

Table S2: Crystal data and structure refinement details for **PdL_2-PdL_4**

Parameter	**PdL_2**	**PdL_3**	**PdL_4**
Empirical formula	C14H9ClN4OPd	C15H10ClN3OPd	C19H12ClN3OPd
Formula weight	391.10	390.11	440.17
Temperature (K)	100.05	100.05	100.15
Wavelength (Å)	0.71073	0.71073	0.71073
Crystal system	Triclinic	Monoclinic	Monoclinic
Space group	P -1	P 21/ c	P n
Unit cell dimension			
a (Å)	8.8485(6)	17.9471(14)	4.5553(3)
b (Å)	10.7306(8)	4.5613(4)	18.3946(9)
c (Å)	15.2015(11)	17.8033(14)	9.1957(4)
α (°)	88.126(3)	90	90
β (°)	74.988(3)	114.681(4)	94.978(2)
γ (°)	69.294(3)	90	90
Volume ($Å^3$)	1301.30(16)	1324.28(19)	767.63(7)
Z	4	4	2
Density (Mg/m^3)	1.996	1.957	1.904
Absorption coefficient (mm^{-1})	1.634	1.603	1.395
F(000)	768.0	768	436.0

Table S3: Selected bond lengths [Å] and bond angles [˚] for **PdL_2-PdL_4**

Bond lengths [Å]			
	PdL_2	**PdL_3**	**PdL_4**
Pd(1)-N(3)	2.0132(19)	2.0168(16)	2.044(9)
Pd(1)-N(1)	2.0136(19)	2.0229(16)	2.095(8)
Pd(1)-N(2)	1.9608(19)	1.9802(15)	1.962(8)
Pd(1)-Cl(1)	2.3191(6)	2.3152(5)	2.326(2)
Bond angles [˚]			
N(3)-Pd(1)-N(1)	164.31(8)	164.12(6)	162.4(3)
N(3)-Pd(1)-N(2)	82.86(8)	82.46(6)	81.3(3)
N(1)-Pd(1)-N(2)	81.45(8)	81.67(6)	81.1(3)
N(3)-Pd(1)-Cl(1)	97.89(6)	97.69(5)	91.5(3)
N(1)-Pd(1)-Cl(1)	97.80(6)	98.19(5)	106.1(2)
N(2)-Pd(1)-Cl(1)	179.25(5)	179.73(5)	171.7(3)

19. Selected computational information

Table S4: Summary of selected computational data for **PdL_1-PdL_4**

Properties	**PdL_1**	**PdL_2**	**PdL_3**	**PdL_4**
Natural bond orbital (NBO) charge				
Pd^{2+}	0.348	0.365	0.340	0.359
O^-	0.392	0.348	0.355	0.357
Bond lengths (Å)				
Computed Pd-Cl	2.444	2.433	2.439	2.466
X-ray Pd(1)-Cl(1)	-	2.3191(6)	2.315(5)	2.328(2)
HOMO-LUMO energy / eV				
- LUMO	3.178	2.979	2.517	2.312
- HOMO	6.246	6.125	6.030	5.826
$\Delta E_{LUMO–HOMO}$	3.068	3.146	3.513	3.514
Chemical hardness (η)	1.534	1.573	1.757	1.757
Electronic chemical potential (-μ)	4.711	4.553	4.274	4.069
Electrophilicity index (ω)	7.233	6.589	5.199	4.711
Dipole moment (Debye)	7.249	5.956	2.529	1.816

20. Concentration dependant Table

Table S5: Average values of k_{obs} (s^{-1}) for **PdL_1**

[Nu]	$k_{obs, s^{-1}}$		
	Tu	**L-Met**	**5'-GMP**
0.002	190.4	101.4	17.8
0.004	380.4	205.2	35.08
0.006	570.2	309.6	51.76
0.008	770.64	408	70.48
0.01	960.2	514	89.3

Table S6: Average values of k_{obs} (s^{-1}) for **PdL_2**

[Nu]	$k_{obs, s^{-1}}$		
	Tu	**L-Met**	**5'-GMP**
0.002	67.2	35.78	6.3
0.004	135.4	73.56	12.7
0.006	200.6	112.34	18.1
0.008	271.8	145.12	24.2
0.01	344.1	182.9	30.3

Table S7: Average values of k_{obs} (s^{-1}) for **PdL_3**

[Nu]	$k_{obs, s^{-1}}$		
	Tu	**L-Met**	**5'-GMP**
0.002	51.262	25.82	4.308
0.004	103.524	51.8	8.592
0.006	150.786	78.76	12.899
0.008	200.048	101.68	17.8
0.01	250.31	128.6	21.61

Table S8: Average values of k_{obs} (s^{-1}) for **PdL_4**

[Nu]	$k_{obs, s^{-1}}$		
	Tu	**L-Met**	**5'-GMP**
0.002	20.902	11.068	1.692
0.004	41.404	20.386	3.394
0.006	59.906	31.294	5.406
0.008	79.908	41.372	6.908
0.01	102.01	51.74	8.606

21. Temperature dependant Table

Table S9: Temperature dependence of k_2 $M^{-1}s^{-1}$ for **PdL_1**

1/T, K^{-1}	In(k_2/T)		
	Tu	**L-Met**	**5'-GMP**
0.00336	5.7648	5.1541	3.3655
0.0033	5.9361	5.3191	3.5121
0.00325	6.1308	5.5071	3.7129
0.00319	6.3097	5.7139	3.9002
0.00314	6.5091	5.8991	4.1129

Table S10: Temperature dependence of k_2 $M^{-1}s^{-1}$ for **PdL_2**

	In(k_2/T)		
1/T, K^{-1}	**Tu**	**L-Met**	**5'-GMP**
0.00336	4.7208	4.1404	2.3148
0.0033	4.9301	4.3617	2.5221
0.00325	5.0991	4.5567	2.7097
0.00319	5.3221	4.6987	2.9121
0.00314	5.5421	4.8877	3.1446

Table S11: Temperature dependence of k_2 $M^{-1}s^{-1}$ for **PdL_3**

	In(k_2/T)		
1/T, K^{-1}	**Tu**	**L-Met**	**5-GMP**
0.00336	4.4347	3.7853	1.9763
0.0033	4.6612	3.9774	2.1754
0.00325	4.9452	4.1689	2.3596
0.00319	5.1375	4.3734	2.5621
0.00314	5.4561	4.5861	2.7683

Table S12: Temperature dependence of k_2 $M^{-1}s^{-1}$ for **PdL_4**

1/T, K^{-1}	In(k_2/T)		
	Tu	**L-Met**	**5'-GMP**
0.00336	3.5116	2.8623	1.1064
0.0033	3.7354	3.0652	1.3468
0.00325	3.9737	3.2654	1.5599
0.00319	4.1892	3.5463	1.7737
0.00314	4.4367	3.6987	1.9734